AN ABSTRACT OF THE THESIS OF

Tingwei Zhang for the degree of Master of Science in Electrical and Computer Engineering presented on November 30, 2020.

Title: Indoor Localization Using Direction of Arrival Approach

Abstract approved: ______________________________

Huaping Liu

In this paper, a Direction of Arrival (DOA) based system is proposed. This method searches the direction relative to the array to find where the signal source is located. The proposed system can achieve sub-meter level accuracy with a near real-time update rate. Also, we introduced several refinement methods including a compact tracking system that is compatible with small items, a DOA accuracy prediction function, a method based on linear prediction to expand antenna array to create a virtual antenna matrix, and a novel method for multipath effect cancellation. Overall, the proposed system achieved sub-meter level accuracy, and the functionality of the refinement methods has been approved in the simulation.

Indoor Localization Using Direction of Arrival Approach

by

Tingwei Zhang

A THESIS

submitted to

Oregon State University

in partial fulfillment of
the requirements for the
degree of

Master of Science

Presented November 30, 2020
Commencement June 2021

Master of Science thesis of Tingwei Zhang presented on November 30, 2020.

APPROVED:

Major Professor, representing Electrical and Computer Engineering

Head of the School of Electrical Engineering and Computer Science

Dean of the Graduate School

I understand that my thesis will become part of the permanent collection of Oregon State University libraries. My signature below authorizes release of my thesis to any reader upon request.

Tingwei Zhang, Author

ACKNOWLEDGEMENTS

Throughout the writing of this thesis I have received a great deal of help and support. I would first like to thank my advisor, Professor Huaping Liu, whose expertise was invaluable in guiding me during my research. Your professional feedback pushed me to improve my thinking and brought my work to a higher level. I would like to express my deepest appreciation to my committee for willing to help me with my defense in short notice. I would also like to thank my colleague Guangxin Wang, for his assistance on acquiring experiment data during my research. Moreover, I would like to give my thanks to my writing consultant Adam Haley form the Graduate Writing Center for helping me through the thesis writing process. In addition, I would like to thank my parents for their support. You are always there for me. Finally, I could not have completed this thesis without the support of my friend, Paris Kalathas, who provided me experience of doing research, as well as happy distraction to rest my mind outside of my research

TABLE OF CONTENTS

TABLE OF CONTENTS (Continued)

Page

LIST OF FIGURES

LIST OF FIGURES (Continued)

Figure Page

LIST OF FIGURES (Continued)

Figure | Page

LIST OF TABLES

Chapter 1: Introduction

Indoor localization is a process that aims to determine the location of a device or user in an indoor setting or environment. In the past few decades, the demand for indoor positioning technologies has rapidly increased, mainly in industrial settings and wireless sensor networks. However, due to the limitations of complex indoor environments, most popular positioning technologies used outdoors such as GPS cannot fulfill the requirements due to the lack of signals and obstacles that cause multipath effects. Since the last decade, there has been a significant scale proliferation of smartphones and wearable devices that are capable of communications; each of these devices can be treated as a signal source that continuously generates electromagnetic waves. Since the electromagnetic wave has a good penetration property against most of the materials in typical indoor environments, it is a good candidate for indoor positioning.

By following this idea, a localization system that is capable of indoor settings and environments based on direction of arrival (DOA) approach is proposed in this thesis. The basic idea of the proposed system is to use a beamforming DOA estimation method to extract signal strength from different arriving angles and find the strongest direction that indicates the direct path of the signal. With two or more antenna arrays placed at different locations, the coordinates of the target can be calculated by using geometry. The proposed system has several advantages: compact size, high accuracy, less computation, and the ability to 'see' through obstacles.

1.1 Background

Positioning technologies can be separated into two categories: indoor and outdoor localization. Common outdoor positioning includes GPS in North America and Galileo in Europe. However, due to the complexity of indoor environments such as obstacles and reflective materials, these technologies cannot be used since the reference signal is corrupted by multipath effects and satellite signals could be too weak. For this reason, indoor localization has become a challenging problem. To solve this problem, various techniques have been proposed in the past, including but not limited to radio frequency signals [1–10], magnetic variation, inertial sensors, images, and laser. Till now, no technology has become dominant in this area.

1.2 Literature Review

Indoor localization technologies have been investigated for the past few decades, but none of them is dominating. Accurate indoor localization is challenging because the properties of indoor environments are extremely complex.

- **Limited area:** Indoor environments are defined as spaces inside buildings, such as rooms or halls. These spaces are surrounded by building materials that can adequately reflect and block common signals, including but not limited to radio waves, infrared, and sound waves. All these reflections will cause the multipath effect and rapidly degrade the performance of existing localization technologies that show high accuracy in the outdoor environment [11].

- **Obstacles:** Within an indoor environment, it is inevitable to have numerous objects exist. Since indoor localization technologies are aimed to track small objects in indoor environments, these obstacles can cover and hide a target object within or behind them. This makes some localization technologies that depend on the Line-of-Sight (LOS) path unable to work.

For a localization system used for indoor environments,there are some requirements that technologies should fulfill in order to become a dominant in this area:

- **Size:** As discussed above, indoor environments are limited in size. This requires any system that attempts to perform localization to have a compact size that will not interfere with the functionality of the environment itself

- **Latency:** For indoor environment localization, it is important to have the ability to track moving objects in real-time. This requires technologies to not be computation consuming.

Because of all these limitations and requirements, although a few techniques have claimed the ability to solve the indoor localization problem [12], it is still not sufficient to become dominant in this area. In this section, some commonly used technologies will be introduced, including the working theory, advantages, and disadvantages.

1.3 Visible Light Localization

Visible light-based localization systems such as visible LED lights based indoor positioning system [13] use light sensors to detect the location of objects. The advantage of visible light is that it can provide high accuracy. However, the visible light-based system performance is limited in indoor environments since obstacles can block visible light. Therefore, non-line-of-sight (NLOS) devices will not be detected.

1.4 RFID

Radiofrequency identification (RFID) is a conventional tracking technology that can be employed for indoor localization applications [14,15]. An RFID-based system consists of a reader that communicates with tags. Readers receive data from tags that are predefined by protocol. There are mainly two types of RFID systems: passive and active. An active RFID system requires tags to connect to the power source to transmit data continuously. The effective range for the system can go up to a hundred meters between tag and reader. However, the accuracy that system can provide is not sufficient for indoor localization purposes. Passive RFID systems can operate without a battery and provide high accuracy. However, the effective range is limited (1-2m), making the system not the right candidate for indoor localization purposes.

1.5 Received Signal Strength Indicator (RSSI)

Received signal strength (RSS) based localization technologies [16–18] are conventional and straightforward methods for indoor localization. The RSS is the actual signal power that is received by the receiver. Usually, RSS is measured in decibel milliwatts (dBm) or milliwatts (mW). RSS can indicate the distance between the signal transmitter (Tx) and receiver (RX). Higher RSS means the distance between TX and RX is small. The accurate distance between TX and RX can be calculated using several different propagation models given a known transmission power or a known RSS at a reference point. RSSI is the RSS indicator, a relative measurement of RSS usually defined by device manufacturers. With RSSI and the signal propagation path loss model, the distance between TX and RX can be calculated from (1.1) as

$$RSSI = P_0 - 10n \log_{10}\left(\frac{d}{d_0}\right) \tag{1.1}$$

where d is the distance of the device from the receiver,p_0 is the received power at reference distance d_0, and n is the path loss component. RSSI-based localization systems usually require at least three reference points to compute the TX location by using geometry or trigonometry. Although the RSSI-based system is simple and lower in complexity and cost, it comes at the expense of poor accuracy. Especially in Non-line-of-sight scenarios, the performance of RSS based systems will be rapidly degraded due to additional signal attenuation caused by propagation through large obstacles such as walls and severe signal interference such as multipath fading effect and indoor noise. Some filters and mechanisms can be applied to mitigate these effects. However, it will come at the expense of using complex algorithms.

1.6 Fingerprinting

Fingerprinting based localization systems usually require environment research to acquire fingerprints of the space where the system is deployed. Initially, the fingerprints for points in the environment are collected and stored in a database during the off-line stage. After the system is deployed, the measurements at the on-line stage will be compared with off-line measurements stored in the database to estimate the location of the device. Usually, fingerprints use channel state information (CSI) or RSSI [19]. Several methods and algorithms are available to match the measurement with the database; one of the most common methods that use probability is discussed below [20].

Probabilistic methods rely on the likelihood that the user is at a location. Assume a set of locations with n candidates is $L = L_1, L_2, L_3, ..., L_N$. For an RSSI value measured as O, the location can be decided as L_i if

$$P(L_i|O) > P(L_j|O), \text{ for } i, j = 1, 2, 3, ..., n \tag{1.2}$$

where i and j denote the different locations. Equation (1.2) shows that the device's location can be classified at L_i if the possibility at i is higher than at any other location.

Although the fingerprinting based localization system is simple and requires less computation, it usually comes at the expense of rapidly increasing the difficulty in system set-up and maintenance.

1.7 Time of Arrival (TOA)

Time of arrival (TOA) or Time of Flight (TOF) based systems measure the signal propagation time to calculate the distance between TX and RX. The distance between TX and RX shown in Figure 1.1 can be calculated by multiplying TOA and the speed of light [21, 22]. In most TOA systems, a minimum of three reference points is required to calculate the device's location using geometry.

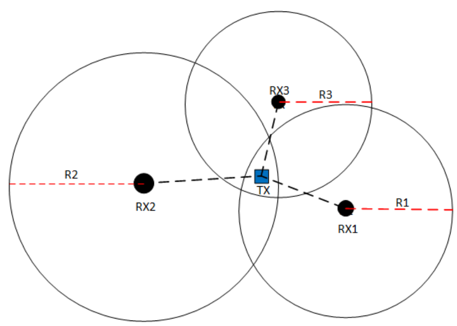

Figure 1.1: TOA localization system

TOA-based localization systems require strict synchronization between TX and RX. The key factors that can affect TOA-based systems' accuracy are the sampling rate and bandwidth of the transmitted signal. The resolution of TOA-based systems is defined by bandwidth with Equation (1.3).

$$R = \frac{c}{2B} \tag{1.3}$$

A low sampling rate reduces the accuracy of the system since the signal may arrive between sampling intervals. Although Ultra-Wideband (UBW) technologies and high sampling rates can help improve the accuracy of TOA based systems [3, 4, 23–30], there is still significant localization error caused by the multipath effect when the system is used for indoor environments. This is because, in indoor environments, the obstacle on the direct path will reflect the signal. As a result, the signal will go through a longer path, causing the TOA to increase, which will significantly increase the distance between TX and RX.

1.8 Time Different of Arrival (TDOA)

TDOA-based localization systems are an improved version of TOA-based methods. Instead of exploiting the time of arrival, TDOA-based systems exploit the signal arrival time difference between receivers. The TDOA measurements are converted to the physical distance difference of TX between two RX [31]. Then the location of the device can be calculated using Equation (1.4)

$$\sqrt{(x-x_1)^2+(y-y_1)^2}-\sqrt{(x-x_3)^2+(y-y_3)^2}=c(t_1-t_3) \tag{1.4a}$$
$$\sqrt{(x-x_2)^2+(y-y_2)^2}-\sqrt{(x-x_3)^2+(y-y_3)^2}=c(t_2-t_3) \tag{1.4b}$$

Unlike the system based on TOA, TDOA doesn't require the absolute propagation time. In this case, the synchronization between transmitter and receiver is no longer necessary [20]. Thus, compared to TOA-based systems, it is easier to deploy. However, to measure the time difference between receivers, synchronizations between all receivers are still required.

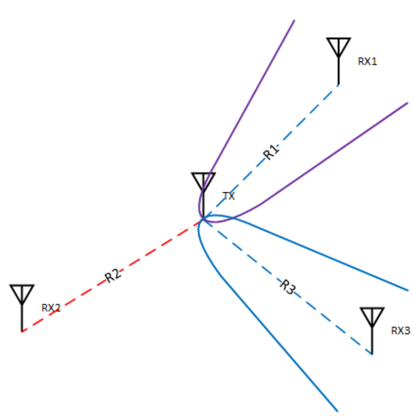

Figure 1.2: TDOA system

1.8.1 Summary

Overall, the existing indoor localization technologies are not sufficient to fit all the requirements; methods that have high accuracy come at the expense of high implementation difficulty. With low implementation difficulty methods, it usually comes at the expense of low accuracy.

Method	Advantages	Disadvantages
Visible Light communication	High accuracy, easy to implement	not suitable for NLOS scenario
RFID	low implementation difficulty,low cost,high accuracy	low effective range, must be near reader
Received Signal Strength Indicator(RSSI)	Easy implementation,low cost	Low accuracy 5-10 meters
Fingerprinting	Easy to use,low system complexity	high implementation difficulty, need fingerprint data in every possible location
Time of arrival	High accuracy(can go up to centimetre level)	High cost,strict synchronization required between tag and receiver
Time difference of arrival	Does not require synchronization between tags and receiver,high accuracy	requires synchronization between receivers

Table 1.1: Common methods pros and cons

Chapter 2: Materials and Methods

2.1 Proposed Method

In this paper, a Direction of Arrival (DOA) based system is proposed. This method searches the direction relative to the array to find where the signal source is located. The advantage of DOA approaches compared with the time-based approaches is that since the determination of DOA is based on phase differences between received signals from different antennas, it does not require synchronization between receivers to calculate the location of the object [20]. Also, DOA approaches can distinguish different signals, which makes this a competitive candidate for indoor positioning applications.

2.1.1 Advantages Over Existing Works

An optimal solution to indoor localization would be accurate (i.e., decimeter-level accuracy), easy to deploy (without requiring complex synchronization cables or power-hungry hardware), and universal (works even in the presence of other RF-based communication devices). As such, the advantages of the proposed scheme for the application are as follows:

- A DOA-based scheme does not require anchor-to-anchor synchronization, making it easy to deploy;
- The technology requires fewer anchors to cover the same area as existing schemes, making it considerably easier to maintain;
- It is highly accurate with 20MHz RF bandwidth (a small fraction of UWB signal bandwidth), minimizing the potential for interference with other wireless communication hardware.

2.1.2 The Goal of the Proposed Method

The indoor localization system's performance can be evaluated in three parts: accuracy, latency, and size of the system. For accuracy, in past works, it varied from decimeter level to meter level. However, typical indoor environments nowadays have a size of around 5 to 10 meters. For this case, meter level error in indoor localization systems is not acceptable. Therefore, the proposed method should have accuracy at least decimeter level (<100cm), ideally less than 20 centimeter. Since the proposed method determines the angle at which signal arrives at the antenna array, the maximum error then can be converted to an angle by using equation (2.1), assuming that the effective range of the system is 5 meters.

$$\max a = \arctan\left(\frac{a}{c}\right) = \arctan\left(\frac{1}{5}\right) = 11.58^\circ \tag{2.1}$$

where a denotes the maximum error of the system, which should be less than 1 meter, and c denotes the system's effective range.Therefore,for the proposed method, the error should not be higher than 11.58°.

2.2 Theory

In this section, the proposed method will be introduced, which includes the physical and mathematical models.

2.2.1 Direction of Arrival Estimation

DOA estimation is a specialized signal estimation technique that uses a phased antenna array to distinguish the signal from different directions. The DOA estimation system can be decomposed into three parts: signal source, receiver with an antenna array, and signal parameter estimation. These three parts can also be separated into three different stages: target, observation, and estimation stage.

- **Target Stage** is the stage when signal sources transmit signals. During this stage, the complex environment creates unknown signal parameters for the DOA estimation system.

- **Observation Stage** is the stage that receives signals from the target stage. Because of the environment's complexity, the received signal usually contains multiple signal parameters such as arriving angle, distance, polarization, and some parameters from the environment, such as noise, interference, and miscellaneous waves.

- **Estimation Stage** is the stage when the DOA estimation technique is applied to the signals from the observation stage. The signal parameters are extracted in this stage. The estimation stage can be treated as a reconstruction of the target stage. The accuracy of this stage is determined by multiple factors: the complexity of the environment, difference between channels, and mutual coupling of the phased array.

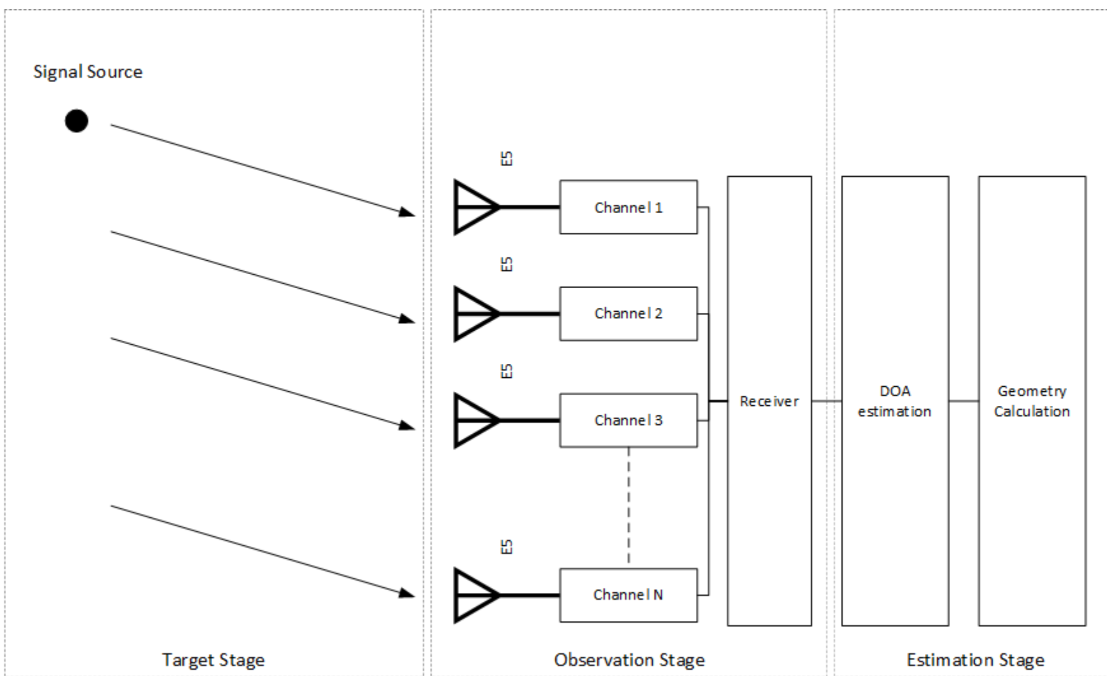

Figure 2.1: DOA estimation system structure

2.2.2 Receiving Angle and Phase Change

The received signal at the receiver is a linear combination of multipath reflection from different directions in free space. Each signal from a specific angle corresponds to a phase shift. To see this, consider the signal received by a 1-D antenna array along the x-axis. Each antenna is separated by distance D, as figure 2.2 shows.

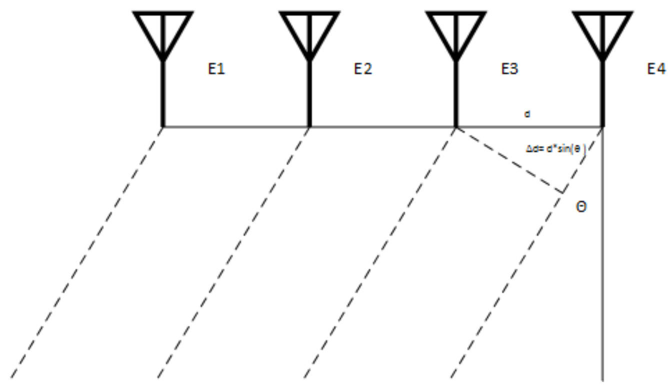

Figure 2.2: Received signal phase change

The phase shift of the signal between the first antenna and the nth antenna corresponds to the extra distance that signal traverses. Then there is a time delay between received signals from the first antenna and the nth antenna which can be expressed as:

$$\tau = \frac{d \sin \theta}{c} \tag{2.2}$$

where d is the distance between antennas, θ is the incident angle of far field signal, and c is the speed of light. Thus, the phase shift due to the time delay between antennas can be obtained as

$$\phi = e^{jw\tau} = e^{jw\frac{d \sin \theta}{c}} = e^{j2\pi f \frac{d \sin \theta}{\lambda f}} \tag{2.3}$$

where f is the central frequency of the signal and λ is the signal wavelength. Therefore, for the narrowband signal, the phase shift between antennas is given as:

$$\phi = e^{j2\pi \frac{d \sin \theta}{\lambda}} \tag{2.4}$$

In order to use the theory described above, the following assumptions are used:

- Point signal source. Assume that a point source is used as a signal source. When looking from the array, the direction of the signal source is unique.
- Narrowband signal. This assumption ensures that all elements in the array can receive signals at the same time.
- Array. The array is assumed to be placed at the far-field region of the signal source. Then the radio wave received by the array can be considered as a plane wave. Also, assuming the position of elements on the array is accurate, the gain and the phase is consistent, it ensures that there is no error from the array
- Noise. Assuming there is no noise between array elements, the noise in the received signal is Gaussian white noise, which is statistically independent.

Under these assumptions, the received signal model can be written as

$$\boldsymbol{x} = \boldsymbol{A}\boldsymbol{s} + \boldsymbol{n} \tag{2.5}$$

Where x denotes the received signal from the receiver, A is the steering vector matrix that indicates the signal phase difference between antennas, s is the source signal, and n is the noise component Then this signal model can be written in matrix form

$$\begin{bmatrix} \boldsymbol{x_1(t)}^T \\ \boldsymbol{x_2(t)}^T \\ \ldots \\ \boldsymbol{x_N(t)}^T \end{bmatrix} = \begin{bmatrix} \boldsymbol{\alpha}(\theta_1) & \boldsymbol{\alpha}(\theta_2) & \ldots & \boldsymbol{\alpha}(\theta_D) \end{bmatrix} \begin{bmatrix} \boldsymbol{s_1(t)}^T \\ \boldsymbol{s_2(t)}^T \\ \ldots \\ \boldsymbol{s_N(t)}^T \end{bmatrix} + \begin{bmatrix} \boldsymbol{n_1(t)}^T \\ \boldsymbol{n_2(t)}^T \\ \ldots \\ \boldsymbol{n_N(t)}^T \end{bmatrix}$$

2.2.3 Existing DOA Algorithms

In the past few decades, several DOA algorithms have been proposed and can be distinguished into two categories: subspace methods and beamforming methods [32–36].Subspace methods (i.e.MUSIC and ESPRIT algorithm) decompose signals into Eigenvalues and Eigenvectors [37–39]. By sorting Eigenvalues in decreasing order, the corresponding Eigenvectors which have the largest eigenvalues will be the signal subspace.

Thus, by reducing the noise, signal parameters such as direction of arrival can be obtained. Beamforming methods(i.e. MVDR and Bartlett algorithm) are one technique that applies weight factors on each element in the antenna array to create a specific radiation pattern [40,41]; this will amplify signals from the desired direction and discard signals from any other direction. After beamforming, the received signal $\boldsymbol{y}$ corresponding to signal source $\boldsymbol{x}$ can be expressed as

$$\boldsymbol{y} = \boldsymbol{w}^H \boldsymbol{x} \tag{2.6}$$

By selecting each weight factor w, the received signal $\boldsymbol{y}$ contains the signals from different directions.

2.2.3.1 MUSIC

The Multiple Signal Classification(MUSIC) algorithm is a high-resolution DOA estimation technique published by Schmidt in 1977 [42]. It is capable of estimating the signal's direction of arrival and also the number of signals. This method decomposes the received signal covariance matrix into signal and noise subspace. The direction of the source can be calculated by steering vectors, which are orthogonal to noise subspace. The mathematical model of the MUSIC algorithm can be described as below:
Assuming there are D signals received by an N element antenna array and D is the number of signal eigenvalues and eigenvectors, the number of noise eigenvalues and eigenvectors is $N - D$.Assuming signal and noise are uncorrelated, the signal correlation matrix is given by:

$$\boldsymbol{R_{XX}} = E\left[(\boldsymbol{AS} + \boldsymbol{N})(\boldsymbol{AS} + \boldsymbol{N})^H\right] \tag{2.7}$$

$$\boldsymbol{R_{XX}} = \boldsymbol{A}E\left[\boldsymbol{SS}^H\right]\boldsymbol{A}^H + E\left[\boldsymbol{R_{NN}}^H\right] \tag{2.8}$$

$$\boldsymbol{R_{XX}} = \boldsymbol{AR_{SS}A}^H + \boldsymbol{R_{NN}} \tag{2.9}$$

where $\boldsymbol{R_{NN}}$ is the noise correlation matrix, which is given by

$$\boldsymbol{R_{NN}} = \delta^2 \boldsymbol{I} \tag{2.10}$$

Therefore, the computed correlation matrix function along with noise is given as

$$= \boldsymbol{A}\boldsymbol{R_{SS}}\boldsymbol{A}^H + \delta^2\boldsymbol{I} \tag{2.11}$$

where $\boldsymbol{A}$ is a $N \times D$ steering matrix, which is given by

$$\boldsymbol{A} = [\boldsymbol{\alpha}(\theta_1), \boldsymbol{\alpha}(\theta_2), ..., \boldsymbol{\alpha}(\theta_D)] \tag{2.12}$$

$\boldsymbol{R_{SS}}$ is a $D \times D$ source signal correlation matrix, which is given by

$$\boldsymbol{R_{SS} = [s_1, s_2, ..., s_D]\,[s_1, s_2, ..., s_D]^T} \tag{2.13}$$

The correlation matrix function then can be decomposed and results in D Eigenvalues corresponding to signal subspace and $N - D$ Eigenvalues that correspond to noise subspace:

$$\boldsymbol{R_{XX}} = \boldsymbol{V_S}\boldsymbol{\Lambda}\boldsymbol{V_S}^H + \boldsymbol{V_N}\boldsymbol{\Lambda}\boldsymbol{V_N}^H \tag{2.14}$$

Since the MUSIC algorithm found the orthogonality relationship between the source victor $\boldsymbol{\alpha}(\theta_n)$ and noise subspaces, therefore,

$$\boldsymbol{\alpha}^H(\theta_n)\boldsymbol{V_N} = 0 \tag{2.15}$$

The spatial spectrum of the signal P_{MUSIC} then can be expressed as a function of θ

$$P_{MUSIC} = \frac{1}{\boldsymbol{\alpha}^H(\theta)\boldsymbol{V_N}\boldsymbol{V_N}^H\boldsymbol{\alpha}(\theta)} \tag{2.16}$$

2.2.3.2 ESPRIT

ESPRIT is short for the Estimation of Signal Parameters via Rotational Invariance Technique, which was introduced by Richard Roy and Thomas Kailath in 1989 [43]. It is another method based on subspace DOA estimation [44–48]. However, ESPRIT does not require searching for all possible steering vectors to estimate DOA, which can rapidly decrease computation and storage resources compared with the MUSIC algorithm by requiring the antenna array to possess displacement invariance. The ESPRIT algorithm is based on the rotational invariance property of the signal subspace. Unlike the MUSIC algorithm, in ESPRIT, the antenna array is decomposed into several sub-arrays as shown in figure 2.3. Consider there is M element antenna array which is divided into two sub-

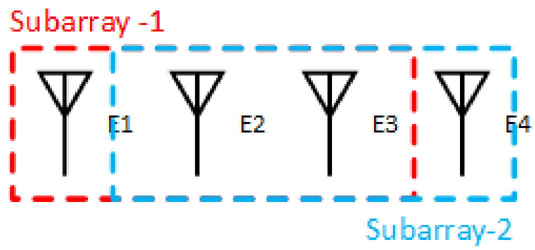

Figure 2.3: Sub-array decomposition

arrays by distance Δ, each sub-array contains $M-1$ elements. Assume there are d far-field incoherent signals received by the array. Signals induced on each sub-array are defined as

$$\boldsymbol{X}_1 = \boldsymbol{A}_1\boldsymbol{S} + \boldsymbol{N} \tag{2.17}$$

$$\boldsymbol{X}_2 = \boldsymbol{A}_2\boldsymbol{S} + \boldsymbol{N} \tag{2.18}$$

$$\boldsymbol{A}_2 = \boldsymbol{A}_1\boldsymbol{\Phi} \tag{2.19}$$

where $\boldsymbol{\Phi} = diag\left\{e^{jw\phi_1}, e^{jw\phi_2}, ..., e^{jw\phi_d}\right\}$, which is a $D \times D$ diagonal unitary matrix with phase shifts, $\phi_i = \frac{2\pi\Delta\sin(\theta_d)}{\lambda}$ between two sub-arrays. The signal subspace of two sub-arrays has been created as V_1 and V_2, then

$$\boldsymbol{V}_1\boldsymbol{\Phi} = \boldsymbol{V}_2 \tag{2.20}$$

Also, a unique non-singular transformation matrix $\boldsymbol{T}$ exists such that

$$\boldsymbol{V}_1 = \boldsymbol{A}\boldsymbol{T} \tag{2.21}$$

$$\boldsymbol{V}_2 = \boldsymbol{A}\boldsymbol{\Phi}\boldsymbol{T} \tag{2.22}$$

where

$$\boldsymbol{T}\boldsymbol{\Phi}\boldsymbol{T}^{-1} = \boldsymbol{\Psi} \tag{2.23}$$

Once $\boldsymbol{\Psi}$ is found, the DOA can be obtained as

$$\theta_i = \arcsin\left(\phi_i \times \frac{\lambda}{2\pi\Delta}\right) \tag{2.24}$$

2.2.3.3 MVDR

The minimum variance distortion-less response(MVDR) method is a typical beamformer proposed by Capon in 1967 [49]. The basic idea of this method is applying a filter to received signal to output signal from the desired direction while minimizing other interference signals. Mathematically, the MVDR can be calculated by the following steps.

$$\min\left\{E\left[\boldsymbol{Y}\boldsymbol{Y}^H\right]\right\} = \min\left\{\boldsymbol{w}^H\boldsymbol{R}_{\boldsymbol{X}\boldsymbol{X}}\boldsymbol{w}\right\} \tag{2.25}$$

In order to keep the signal from direction θ

$$\boldsymbol{w}^H(\boldsymbol{A}(\theta)s(t)^T) = s(t)^T \tag{2.26}$$

$$\boldsymbol{w}^H\boldsymbol{A}(\theta) = 1 \tag{2.27}$$

Where $\boldsymbol{A}$ is the array manifold matrix. The weight vector for beamforming angle θ can be denoted as

$$\boldsymbol{w} = \frac{\boldsymbol{R}_{\boldsymbol{X}\boldsymbol{X}}{}^{-1}\boldsymbol{A}^H(\theta)}{\boldsymbol{A}(\theta)\boldsymbol{R}_{\boldsymbol{X}\boldsymbol{X}}{}^{-1}\boldsymbol{A}^H(\theta)} \tag{2.28}$$

Therefore, the signal power from direction θ

$$P(\theta) = \frac{1}{\boldsymbol{A}(\theta)\boldsymbol{R}_{\boldsymbol{X}\boldsymbol{X}}{}^{-1}\boldsymbol{A}^H(\theta)} \tag{2.29}$$

2.2.3.4 Bartlett

Given the phase difference between two antennas in a two-dimensional antenna matrix as discussed above, if a time delay is added to the received signal that is opposite and equal to the phase change which is caused by the extra transverse distance between antennas, then it will result in all signals from each antenna being in phase perfectly. The sum of these in phase signals will significantly increase the SNR of the signal from the desired angle. This ensures that only the signal from the specified angle can be amplified. Also, adding incorrect time delay to the signal from other undesired directions will destructively interfere with the signal, resulting in a rapidly degraded signal strength, but the correct direction will be amplified as discussed above. The mathematical model of the Bartlett algorithm can be presented as:

$$y(t) = \sum_{n=0}^{N-1} x_n(t) w_n^H = \boldsymbol{W}^H \boldsymbol{X}(t) \tag{2.30}$$

Where $x(t)$ is the received signal from the $n-th$ antenna. N is the number of antennas in the array. The signal power at angle θ:

$$P(\boldsymbol{W}) = \frac{1}{N} \sum_{n=1}^{N} |y(t)|^2 = \frac{1}{N} \sum_{n=1}^{N} \boldsymbol{W}^H \boldsymbol{X}(t) \boldsymbol{X}^H(t) \boldsymbol{W} \tag{2.31}$$

$$\max_{\boldsymbol{w}} E \left\{ \boldsymbol{W}^H \boldsymbol{X}(t) \boldsymbol{X}^H(t) \boldsymbol{W} \right\} = \max_{\boldsymbol{w}} \left\{ E \left| s(t) \right|^2 \left| \boldsymbol{W}^H \boldsymbol{\alpha}(\theta) \right|^2 + \delta^2 \left| \boldsymbol{W} \right|^2 \right\} \tag{2.32}$$

$$\boldsymbol{W}_{BF} = \frac{\boldsymbol{\alpha}(\theta)}{\sqrt{\boldsymbol{\alpha}^H(\theta) \boldsymbol{\alpha}(\theta)}} \tag{2.33}$$

2.2.4 Comparison Between Algorithms

To verify the effectiveness of the algorithms mentioned earlier, we ran simulations for all four algorithms. During the simulation, 30° and 60° signals were combined with Gaussian white noise and fed to all four algorithms. As seen in the figure below, all four algorithms show similar signal strength patterns that have a peak at both 30° and 60°, suggesting that they are good candidates for this project. The difference between all four algorithms is their resolution. As shown in the figure 2.4, the algorithm using the subspace approach generally has a higher resolution than beamforming approaches. The MUSIC algorithm has the highest resolution, and Bartlett beamforming has the lowest resolution among all four methods.

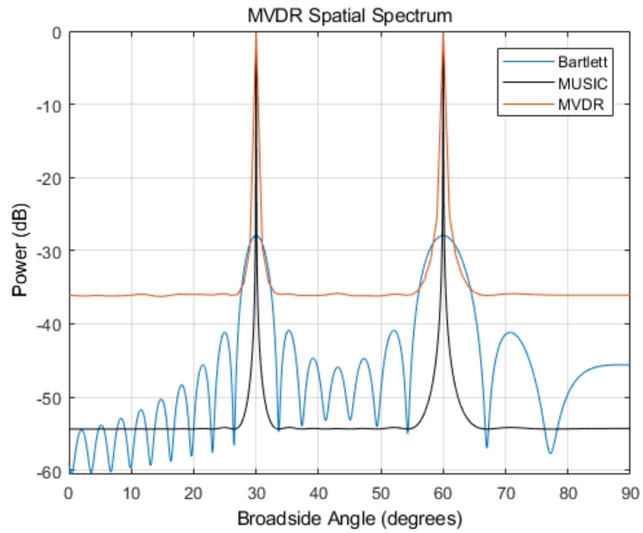

Figure 2.4: DOA algorithms comparison

2.3 Simulation

In this simulation, the signal source was defined as a 5.52GHz sine wave, which is located at 45°. The antenna elements were placed half-wavelength away from each other. Then the signal was modified to simulate the received signal with different amplitude and phase at receivers, and the waveform is shown in figure

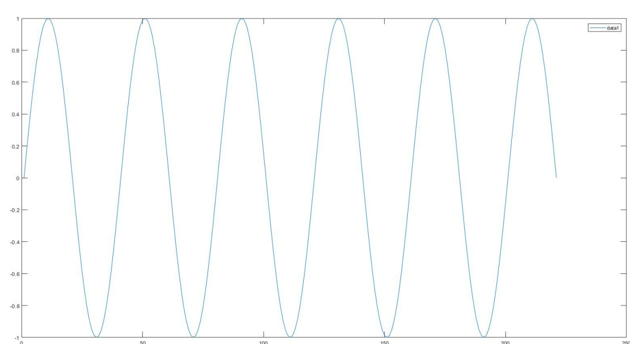

Figure 2.5: Original waveform at 45°

Figure 2.6 below simulated the signal received at array from a source located at 45°

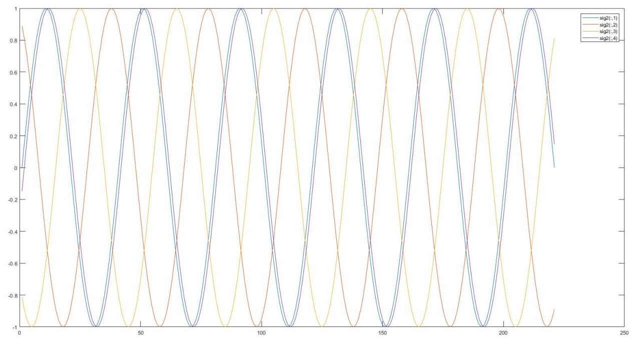

Figure 2.6: Signal arrived from 45°

To simulate the multipath effect in an indoor environment, we added a signal source with a lower amplitude (amplitudes are 10% less than signals at 45°) at 30° in the simulation. The overall waveform is shown in the figure 2.7 below:

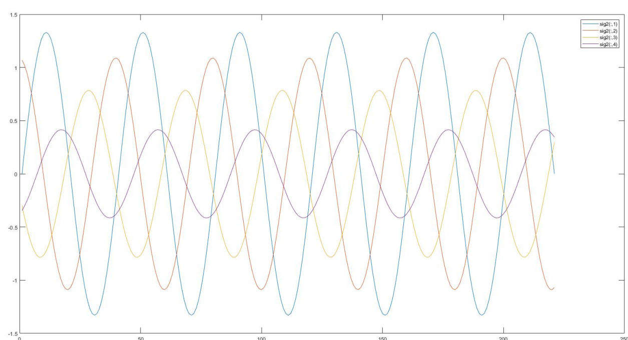

Figure 2.7: Signal after combination and attenuation

After adding the additional signal to simulate the multipath effect, Gaussian white noise with SNR of -20 dB was added to the signal to simulate the worst situation in the real world. The waveform after adding noise is below:

After that, different signal attenuation was applied on the received signal from 30° to simulate different multipath reflections (i.e.First reflection and N-th reflection).

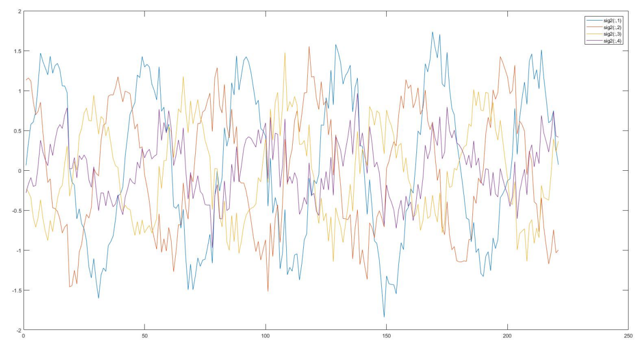

Figure 2.8: Received noise with noise

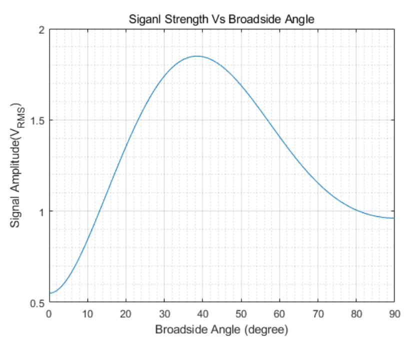

Figure 2.9: Simulation result with 10% attenuation from 30°

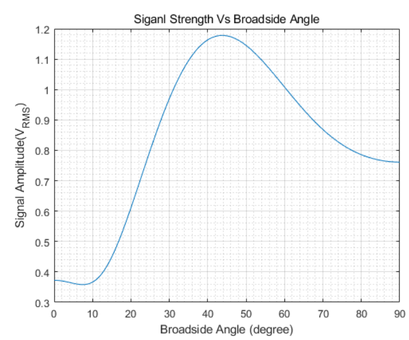

Figure 2.10: Simulation result with 90% attenuation from 30°

Figure 2.9 shows the simulation result for source signal that has been reflected only once with low attenuation(assume 10% loss in this case); the strongest signal was detected at 38°. Figure 2.10 shows the simulation result for source signal that has been reflected multiple times without superposition which has high attenuation(assume 90% loss in this case); the strongest signal was detected at 44°. The simulation result shows that even with low attenuation, the chosen algorithm can still provide a reasonably accurate DOA estimation.

2.3.1 MUSIC Algorithm vs. Bartlett Algorithm Performance

Compared with other algorithms, the Bartlett algorithm is the most accurate one when it is used in the practical environment.Figure 2.11 below is the outcome of all algorithms when applied to the actual received signal, where the signal source was placed at 12.3°. As the result, when the MUSIC algorithm has been used for indoor environment localization, the error is higher than the Bartlett algorithm. This result makes us decide to adapt the Bartlett algorithm as a foundation in this project.

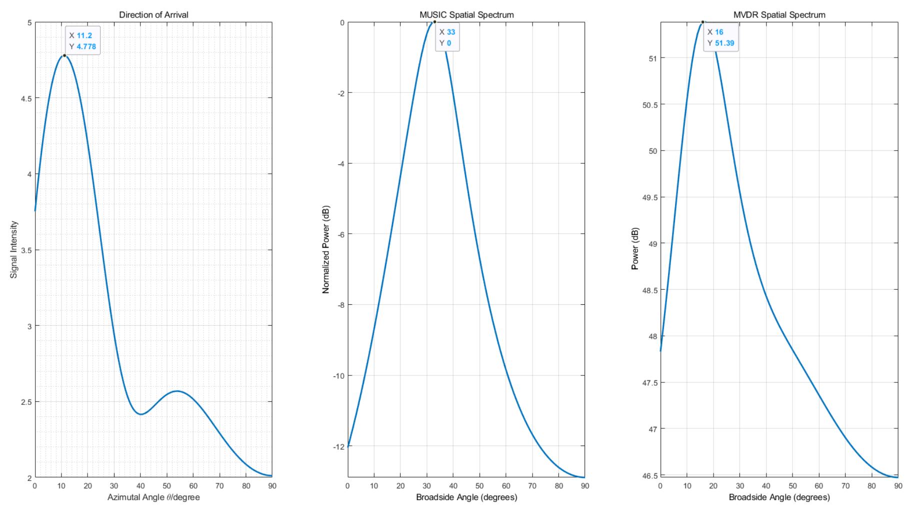

Figure 2.11: Outcome of different algorithms

Chapter 3: Experiment and Analysis

3.1 Hardware Description

In this section, hardware that has been used in the experiment will be introduced, which includes three categories: transmitter, receiver, and antenna array.

3.1.1 Transmitter

During this project, the selected method has been tested in both 2.4G and 5G Wi-Fi environments. As shown in figure 3.1, in the 5GHz Wi-Fi environment, an AD9361 evaluation board from Analog Devices has been used as a transmitter to emit a predefined waveform to free space continuously.

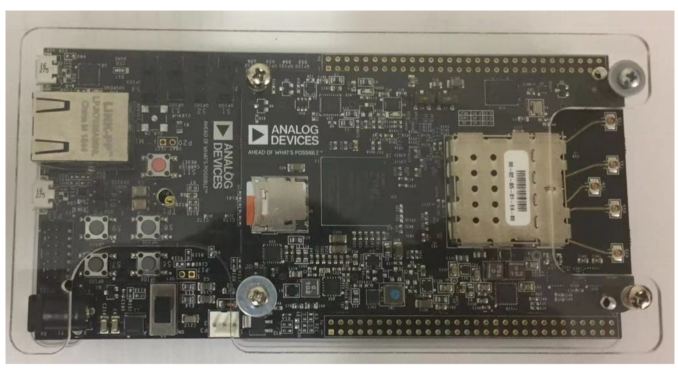

Figure 3.1: Transmitter

In the 2.4GHz Wi-Fi environment experiment, as shown in figure 3.2, an evaluation board based on ESP-8266 has been used as a transmitter. This board has an on-chip system that gives users the ability to predefine the waveform through Arduino.

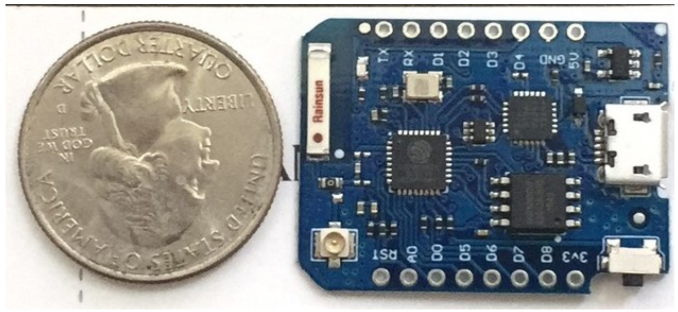

Figure 3.2: Transmitter used in 2.4GHz experiment

3.1.2 Receiver

For this project, as shown in figure 3.3, a data acquisition unit based on the AD9361 transceiver evaluation board has been used as a receiver. This board provides a radio frequency (RF) platform that contains a 16-channel input/output (I/O) interface for 2.4GHz or 5GHz frequency transmitting and receiving(4 channels for each mode). This receiver converts radio frequency signals into baseband signals for further processing. Two receivers were placed at the edge of the test field, as shown in figure 3.4.

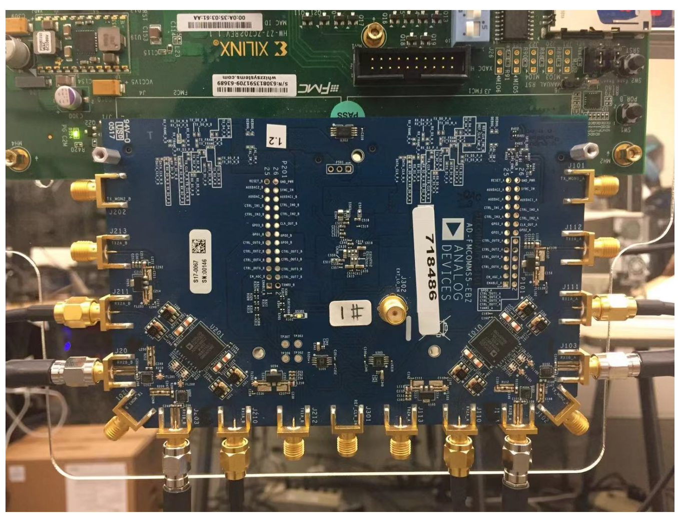

Figure 3.3: Receiver

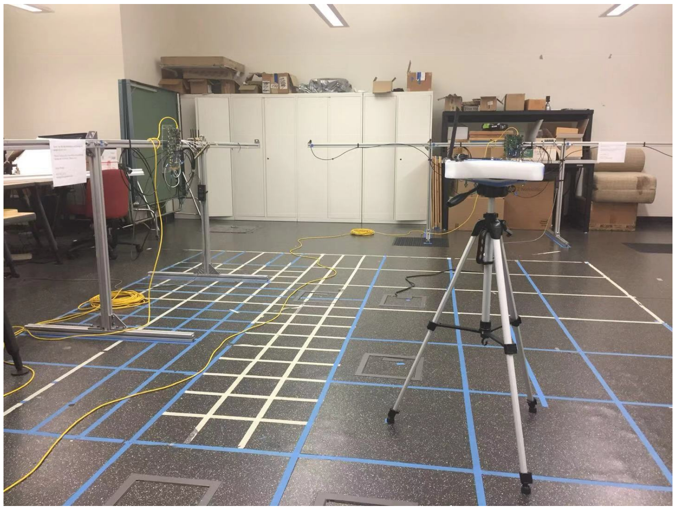

Figure 3.4: Test field

3.1.3 Antenna Array

Since the proposed system in this paper is based on the DOA method, a uniform linear array (ULA) is required for receivers. In this project, since the receivers only support receiving signals from four channels simultaneously, the array was built with four antennas with inter-element distance of half wavelength. For 2.4GHz, the wavelength of the signal is around 10 centimeters, and for 5GHz signal, the wavelength is 5 centimeters. Therefore, the distance between antennas for the 2.4GHz Wi-Fi antenna array should be 5 centimeters and 2.5 centimeters for the 5GHz antenna array, as shown in figure 3.5 and 3.6.

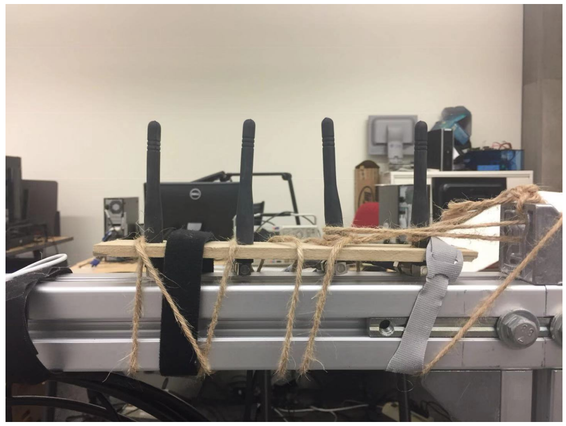

Figure 3.5: Antenna array used in 2.4GHz experiment

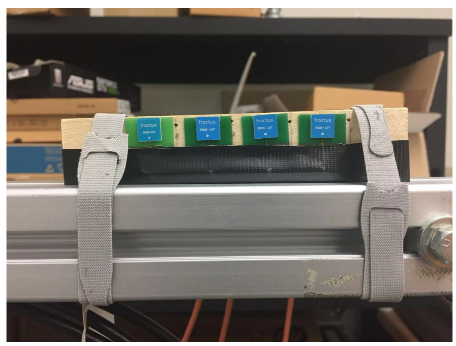

Figure 3.6: Antenna array used in 5GHz experiment

3.2 Experiment

Since the simulation results showed that the proposed system works as expected with reliable accuracy, the system was tested in a realistic environment to evaluate performance in the real world. In this experiment, an AD9341 transmitter was used as a signal source that transmits a signal with 5.52GHz central frequency and 40MHz bandwidth. The set-up location of the transmitter was decided before the experiment, and the theoretical direction of arrival corresponding to the antenna array was calculated. The experiment setup and theoretical angle is shown in figure 3.7 and table 3.1 below.

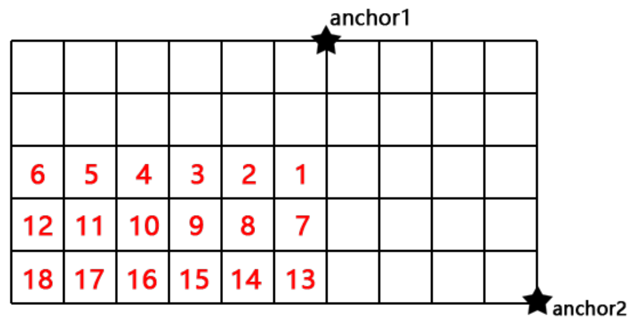

Figure 3.7: Experiment setup

Position	Anchor 1	Anchor 2
1	12.4	27.5
2	31.3	23.2
3	45	20
4	55	17.6
5	61	15.6
6	67.4	14.3
7	8.8	16.5
8	23.36	13.7
9	35.51	11.7
10	44.7	10.2
11	52.4	9
12	59.8	8.1
13	6.7	5.1
14	18.37	4.2
15	28.75	3.5
16	37.81	3.1
17	45	2.7
18	52.88	2.5

Table 3.1: Theoretical angle for each point to both anchor

3.2.1 Experiment Process

The experiments described in this section followed a series of processes that can be separated into three stages: preparation, signal transmitting-receiving, and signal processing.

3.2.1.1 Preparation Stage

During the preparation stage, the following process has been performed: set the receiver, record the original signal from the transmitter, and install the transmitter at the desired location.

At the beginning of the experiment, the receiver's setting was carefully configured, which includes clock frequency and gain of the receiver. This process aims to ensure that the signal can be received at a reasonable amplitude level. If the signal strength is too high, it will be saturated, resulting in adding a high-frequency noise to the signal, which can significantly degrade the performance of the algorithm.

After setting up the receiver, the original signal from the transmitter was recorded, as shown in the figure 3.8. This process aims to ensure that all received signals have a reference to compare; thus, only correct signals will be processed by the algorithm.

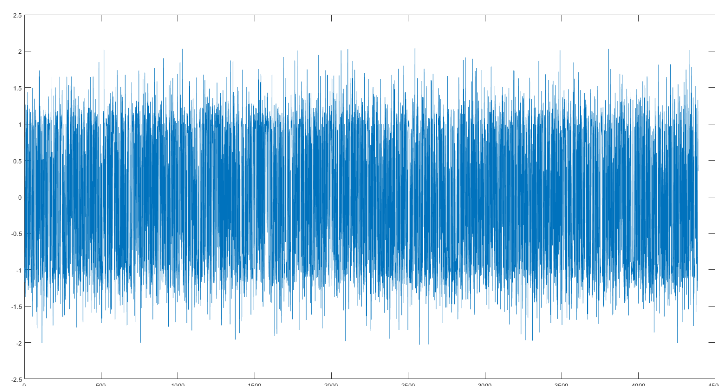

Figure 3.8: Original signal waveform

After configuring the receiver and recording the reference signal, the transmitter was placed at a fixed location determined by the experiment set-up (see figure 3.7). In this way, the theoretical DOA is known and can be used to compare with the estimation result.

3.2.1.2 Signal Transmitting and Receiving Stage

After preparations were finished, the transmitter was connected to omnidirectional antennas. Then the transmitted signal was captured by the receiver. However, before applying the algorithm to captured signals, an identification process is required, as mentioned above. The correlations between reference and captured signals are calculated, as shown in the figure 3.9 below. During this process, any signal with a correlation lower than a certain threshold will be discarded to ensure that only desired signals will be processed.

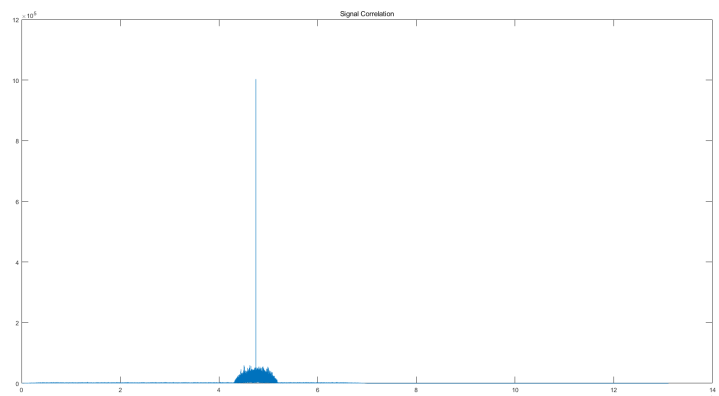

Figure 3.9: Correlation result

3.2.1.3 Signal Processing Stage

The correct signals selected by the last stage were fed to the DOA estimator. After applying the Bartlett algorithm, the DOA of the captured signal was detected, as shown in the figure 3.10 below. Then, the DOA estimation result was used to draw a beam to indicate the direction, as shown in figure 3.11. The dashed line indicates the theoretical DOA, and the solid line indicates the estimated DOA. Then the DOA is fed to the geometry calculation module to convert the DOA into Cartesian coordination.

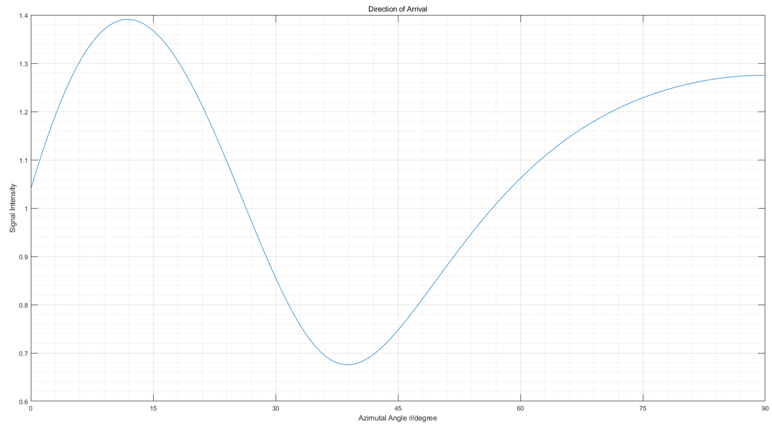

Figure 3.10: DOA estimation example

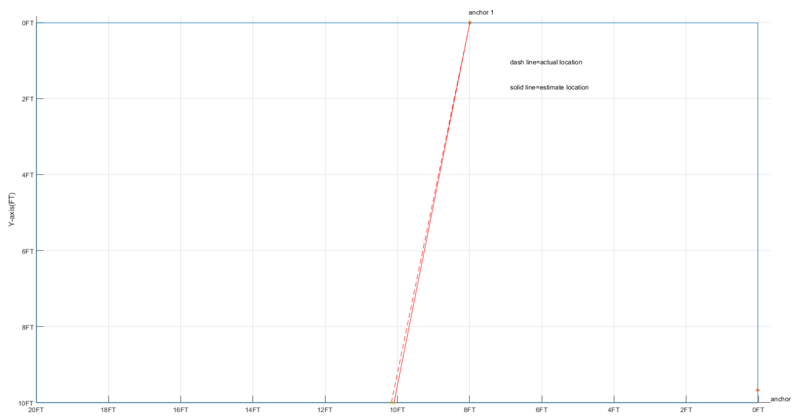

Figure 3.11: DOA indication on a map

3.2.2 First Experiment

In the first experiment, only anchor one was tested with a 4-element ULA antenna array. During the experiment, all 18 points were tested ten times to determine the average value of the arriving angle. Experiment result and error are shown in table 3.2.

The high level of error is not expected since the proposed system has shown reliable

Position	Theoretical(degree)	Average(degree)	Error(degree)
1	12.4	21.7	9.3
2	31.3	44.6	13.3
3	45	66.3	22.3
4	55	40.6	-14.4
5	61	26.6	-34.4
6	67.4	74.8	7.4
7	8.8	19.0	10.2
8	23.36	41.2	17.8
9	35.51	41.6	6.0
10	44.7	59.4	14.7
11	52.4	47.6	-4.8
12	59.8	10.9	-48.9
13	6.7	18.6	11.9
14	18.37	37	18.6
15	28.75	45.1	16.4
16	37.81	54	16.1
17	45	43.4	-1.6
18	52.88	24.4	-28.5

Table 3.2: Average angle and error for each point to anchor 1

accuracy in the simulation. Therefore,we started an inspection of the experiment devices. For the proposed system, a ULA antenna array is required in which all antennas on the array should have the same gain. However, in the first experiment, when the transmitter was placed directly in front of the antenna array, the received signal had a different amplitude level instead of having approximately the same level, to identify the cause of this error, whether it is caused by SMA cable or antenna, the first thing that was checked is the SMA cable. The antennas which have the highest amplitude and lowest amplitude were switched. After switching connection, the waveform showed that the amplitude between these two connections was switched as well.

This result proved that error in the experiment was caused by SMA cable malfunction. For this reason, the SMA cable was changed. Also, to make sure the second experiment can perform better than the first experiment, a series of inspections were applied to all the devices needed in the experiment.

3.2.3 Second Experiment

After inspections and calibrations to all experiment devices, a second experiment was performed. In this experiment, all parameters remained the same as in the first experiment. The result shows that the error has been reduced significantly, with an average error of 4.2°, as shown in table 3.3.

Position	Theoretical	Average	Error	Error(1st)
1	12.4	11.76	1.55	9.3
2	31.3	26.22	1.77	13.3
3	45	54.65	9.65	22.3
4	55	59.46	4.46	14.4
5	61	62.91	1.91	34.4
6	67.4	74.38	6.98	7.4
7	8.8	9.58	0.78	10.2
8	23.36	24.87	1.51	17.8
9	35.51	27.81	-7.7	6.0
10	44.7	48.58	3.88	14.7
11	52.4	50.56	-1.84	4.8
12	59.8	63.96	4.16	48.9
13	6.7	8.99	2.29	11.9
14	18.37	22.24	3.87	18.6
15	28.75	24.42	-4.34	16.4
16	37.81	27.16	-10.65	16.1
17	45	50.45	5.45	1.6
18	52.88	46.81	-6.07	28.5

Table 3.3: Average angle and error for each point to anchor 1

As shown in the result, during this test, all 18 points had an error of less than the 11.58° thresholds. This result proves that the proposed system is capable of indoor localization purposes. The static error analysis will be discussed in section 3.4. Since the system shows the capability of performing indoor localization, a full-scale experiment that simultaneously uses two receivers to estimate transmitter location will be discussed in the next section.

3.2.4 Full Scale Experiment

The second experiment's result proves that the proposed system can identify the direct path between the transmitter and receiver within the indoor environment.We started a full-scale experiment to determine the Cartesian coordinates of the target device. During the experiment, the same experimental procedure was followed as the two experiments before. After acquiring two DOAs, the Cartesian coordination of the transmitter was calculated using geometry. The calculation process is shown below:
for a fixed receiver pair with known location (x_1, y_1) and (x_2, y_2),the length of x-axis and y-axis as x_m and y_m , the distance between two points l_0 can be calculated as

$$l_0 = \sqrt[2]{(y_m - y_1)^2 + (x_m - x_1)^2} \tag{3.1}$$

As figure 3.12 shows, with two receiver points and a potential transmitter location, three points can form a triangle. By using the triangular geometry equations below, the potential transmitters' Cartesian coordination (x_e, y_e) can be calculated with signal receiving angle α_1, α_2as

$$\beta_1 = \arcsin(\frac{x_m - x_1}{l_0}) \tag{3.2}$$

$$\beta_2 = \arccos(\frac{x_m - x_1}{l_0}) \tag{3.3}$$

$$\phi_1 = \alpha_1 + \beta_2 \tag{3.4}$$

$$\phi_2 = \frac{\pi}{2} - \alpha_2 - \beta_1 \tag{3.5}$$

$$l_1 = l_0 * (\sin(\phi_1)/\sin(\pi - \phi_1) - \phi_2) \tag{3.6}$$

$$x_e = x_m - l_1 * \cos(\alpha_2) \tag{3.7}$$

$$y_e = l_1 * \sin(\alpha_2) + y_2 \tag{3.8}$$

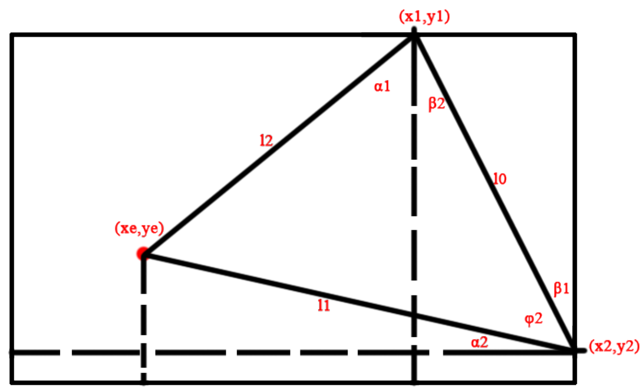

Figure 3.12: Cartesian coordination geometry

3.3 Result

As section 3.2.4 discussed, the experiment for 5GHz Wi-Fi signal environments showed the ability to achieve high accuracy when tracking radio wave emitting devices within the indoor environment. The direction of arrival measurement result for the full-scale experiment is shown in table 3.4

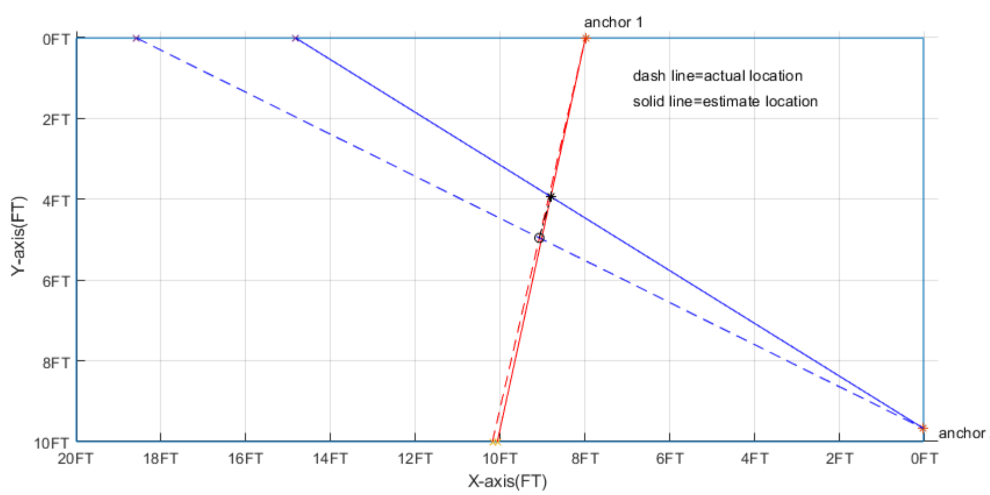

Figure 3.13: Experiment result at Point 1

position	$\alpha_1(r)$	$\alpha_1(e)$	$\alpha_2(r)$	$\alpha_2(e)$
1	12.4	11.76	27.5	33.13
2	31.3	26.22	23.2	25.95
3	45	54.65	20	25.66
4	55	59.46	17.6	25.23
5	61	62.91	15.6	18.71
6	67.4	74.38	14.3	24.15
7	8.8	9.58	16.5	21
8	23.6	24.87	13.7	22.25
9	35.51	27.81	11.7	20.07
10	44.7	48.58	10.2	20.27
11	52.4	50.56	9	22.86
12	59.8	63.96	8.1	16.97
13	6.7	8.99	5.1	6.92
14	18.37	22.24	4.2	19.21
15	28.7	24.42	3.5	13.79
16	37.81	27.16	3.1	15.91
17	45	50.45	2.7	11.58
18	52.88	46.81	2.5	7.66

Table 3.4: Measurement angle for full scale experiment

After the DOA estimation has been converted into Cartesian coordination using equation (3.2) to (3.8), the coordination of the target device has been acquired. Figure 3.13 shows the experiment's visualized result where the transmitter has been placed at point 1; the location estimation of all 18 points has been listed in the table 3.5. As shown in the result, the proposed algorithm can track targets with high accuracy. The mean error of the estimation is 80 centimeters.

The figure 3.14 below shows the visualization result of the estimation of all 18 points, where $*$ indicates the actual location of the emitter, o indicates the estimated location.

3.4 Error Analysis

Although the proposed system shows the ability to track a small object with high accuracy, errors exist in the estimation that cannot be ignored. In order to improve the performance of the system, error analysis has been applied to the result. The error distribution is shown in figure 3.15 and 3.16 for both anchors 1 and 2. The mean error of estimation for anchor 1 is 4.5° with a standard deviation of 2.9°; the mean error of estimation for anchor 2 is 7.9° with a standard deviation of 3.8°. Both error distributions have shown a pattern that is similar to the normal distribution, which means

position	x_{theory}	$x_{estimate}$	y_{theory}	$y_{estimate}$	error
1	333	332.25	152	133.78	33.16
2	273	270	152	120.68	23.49
3	213	197	152	165.4	45.17
4	153	110	152	158.23	66.26
5	93	115	152	196.58	32.08
6	33	35.11	152	212.28	116.93
7	333	328.5	91	91.67	23.8
8	273	281.18	91	110.96	51.37
9	213	247.81	91	99.48	72.86
10	153	166.33	91	124.4	83.06
11	93	203.8	91	136.33	145.18
12	33	14.17	91	128.6	109.17
13	333	334.63	31	44.92	13.7
14	273	288.17	31	79.39	87.59
15	213	253.12	31	68.53	79.07
16	153	211.86	31	76.47	131.04
17	93	93.05	31	94.69	81.3
18	33	121.72	31	55.51	97.26

Table 3.5: Measurement coordinates for full scale experiment

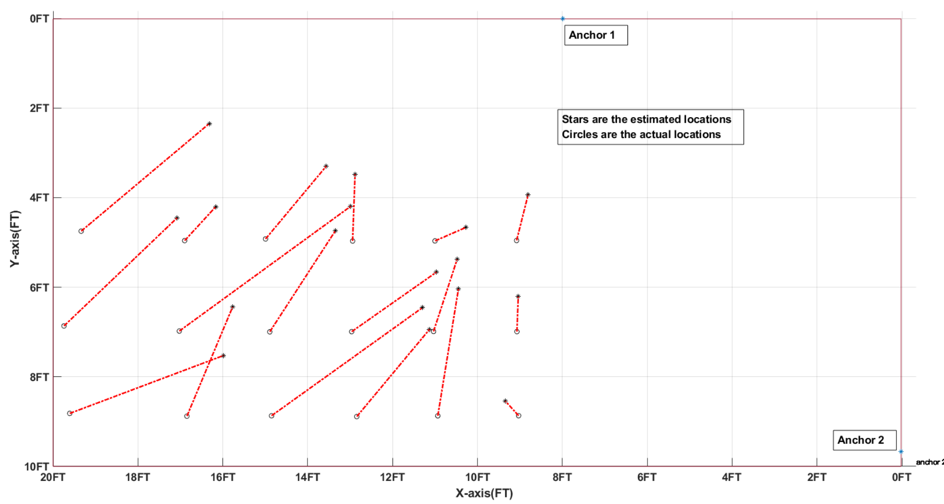

Figure 3.14: Visualized result for 18 points

the error that comes from the proposed system is random due to imperfect calibrated array [50]. However, the errors from anchor two are much higher than anchor one due to the malfunction of receiver two. The other factor that may enlarge the error is that for applying the DOA method, a ULA is required at the receiver, which is usually ideal in theory. However, in reality, because the flaws in hardware are usually allowed by manufacturers, the ULA cannot be as perfect as theory.

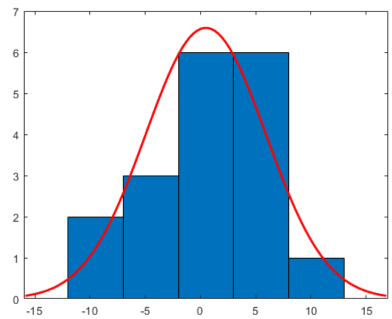

Figure 3.15: Error distribution for anchor 1

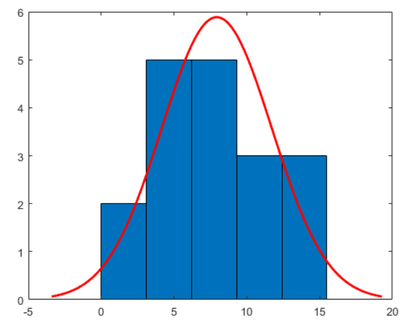

Figure 3.16: Error distribution for anchor 2

The figure below shows the comparison of estimated angle error with actual angle. The result indicates that there is also no connection between actual angle and error. Although the angle errors have no apparent relationship with theoretical angles, after

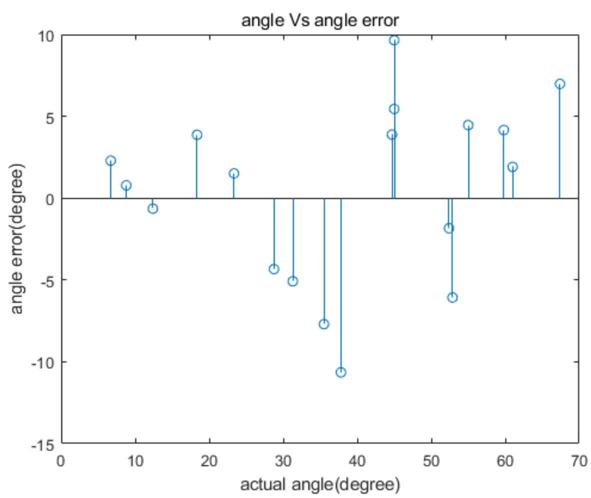

Figure 3.17: Angle error vs. actual angle

converting angle errors into the distance, the result indicates that the relationship between error and distance away from anchor can be expressed as a linear function, as shown in figure 3.18. As the distance between transmitter and receiver increases, the location error will also increase. After performing linear regression to the data, the relationship between error and distance can be expressed as:

$$\epsilon = 0.25d - 0.31 \tag{3.9}$$

Where ϵ is the distance between actual and estimated position and d is the distance between transmitter and receiver. Therefore, the expectation of error for the proposed system at 6 meters away from anchor two will be approximately 1.2 meters, which seems to fail for the goal. However, such colossal error is mainly caused by an error from the estimation of anchor two due to the receiver's malfunction.

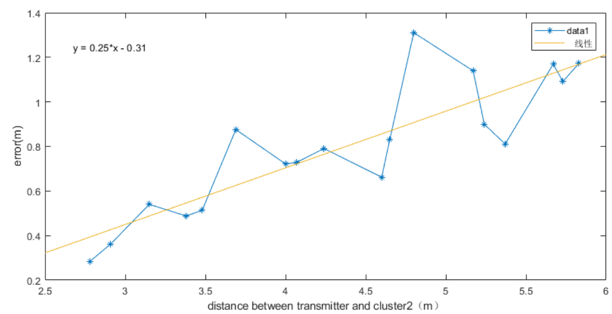

Figure 3.18: Error distance vs. distance between anchor and emitter

Assuming there is no malfunction at receiver 2, the hypothetical error compared with distance can be expressed as figure 3.19. In this case, the linear regression function can be expressed as

$$\epsilon = 0.093d + 0.14 \tag{3.10}$$

The slope of the linear regression function is flatter than the previous figure, which indicates that the impact caused by distance is reduced. Therefore, the expectation of error for the proposed system at 6 meters away from anchor two will be approximately 0.69 meters, which achieves the goal.

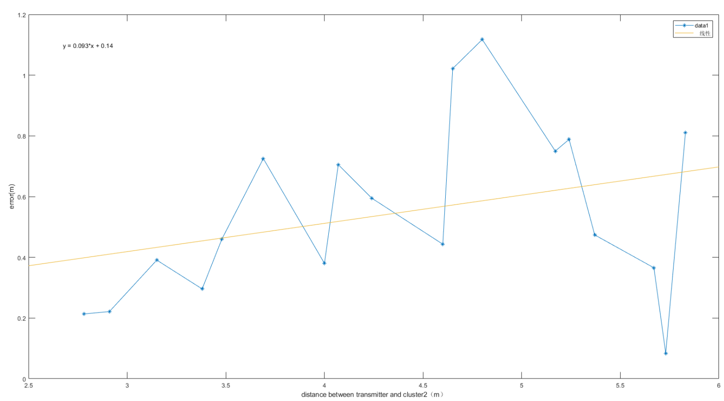

Figure 3.19: Ideal error distance vs. distance between anchor and emitter

Chapter 4: Refinement and Enhancement

In this chapter, we introduce a series of refinement and enhancement methods based on the results of the experiment, aiming to improve the proposed system, which includes four sections: compact tracking system,accuracy prediction of DOA estimation, virtual array expansion, and multipath cancellation method.

4.1 2.4GHz Ultra Low Power Compact Tracking System

As discussed above, the proposed system shows the ability to track an electromagnetic wave transmitting device if the central frequency and waveform are known to the receiver. However, since currently there is no 5GHz programmable compact signal transmitter on the market, lowering the signal's central frequency to 2.4GHz is a choice. The advantage of choosing this frequency range is that compared to the 5GHz device, the 2.4GHz device has a sophisticated environment. The difficulty of acquiring a programmable device with compact size is reduced rapidly. Also, because of the sophisticated environment, Ultra-Low Power consumption has become a regular parameter in this category. In this section, a compact transmitter device with the tracking system introduced above has been built. It is capable of tracking small animals, such as rodents or cats, with long battery life.

Since the signal transmitting frequency has been changed from 5GHz to 2.4GHz, it is necessary to check system performance at each receiver to see if it still can provide similar performance as 5GHz. In this case, the antenna array was rebuilt. The new antenna array at each receiver had an inter-element spacing of 5 centimeters to keep them away at half wavelength. Figure 4.1 and 4.2 are results for the test run on anchor one, where the tags was placed at point 2 and 4.

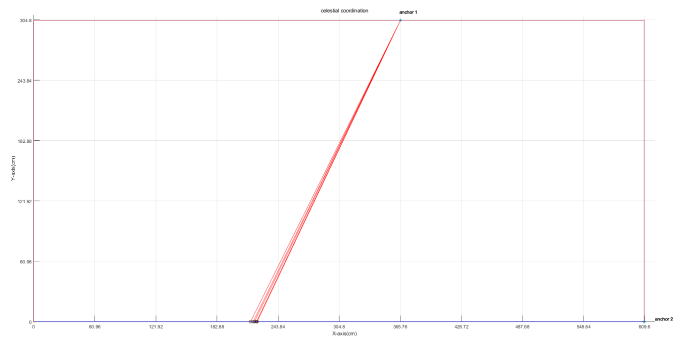

Figure 4.1: Test result at point 2

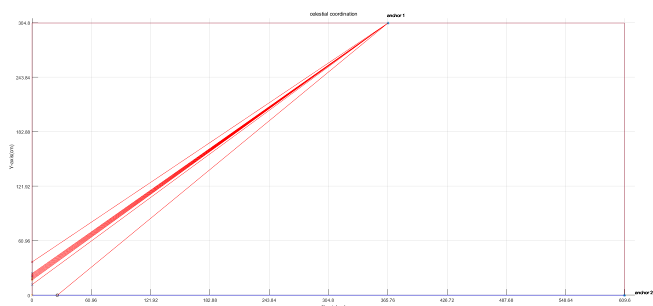

Figure 4.2: Test result at point 4

4.2 Accuracy Prediction Algorithm

In the Bartlett algorithm, several factors can affect its performance such as element number, inter-element space, and SNR [51] . For this reason, we decided to develop a function to predict the accuracy of the Bartlett algorithm using the given parameters; thus, we can configure all parameters accordingly to achieve the highest accuracy in the preparation stage.

4.2.1 Accuracy Definition

In order to research how different parameters will affect the performance of DOA algorithms, in this simulation, the accuracy of the estimation was defined as below:

$$Accuracy = \frac{\#\ of\ estimations\ has\ error\ < threshold}{\#\ of\ total\ etimations} * 100\% \tag{4.1}$$

where the thresholds in this simulation are given as 2°, 5° and 10°.

4.2.2 Simulation Process

During the simulation, for each parameter, 1,000 estimations were performed. While evaluating the impact of each specific factor, all other factors were set to a fixed value. The table below shows default values that were used in this simulation.

Parameters	Element Number	Element Spacing	SNR
Values	8	0.75λ	0 dB

Table 4.1: Constants used in simulation

After simulations, all factors showed the ability to rapidly improve the DOA algorithm's accuracy when they were increased. All these results show that no matter which factor was evaluated, the improvement had a saturation region. Next, we will describe the impact caused by each factor separately.

4.2.3 Element Numbers

The number of elements in the array is a critical factor that can significantly affect the DOA algorithm's performance. Figure 4.3 below is the simulation result for the Bartlett algorithm with different array elements (8,16,32) while other parameters remained the same. In this simulation, the signal sources were located at 15° and 30°. As results show, the resolution of the Bartlett Algorithm increases when the element number increases. However, this improvement is not unlimited. In our simulation, the improvement of accuracy has a saturation region. Once the element number exceeds this limit, there is no additional significant change. As shown in figure 4.4 , the saturation point is 16 elements. The simulation results are also provided in table 4.2 below.

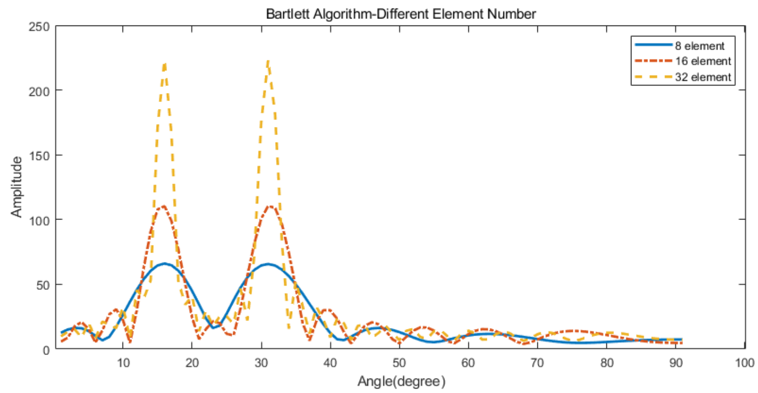

Figure 4.3: DOA estimation performance under different element number

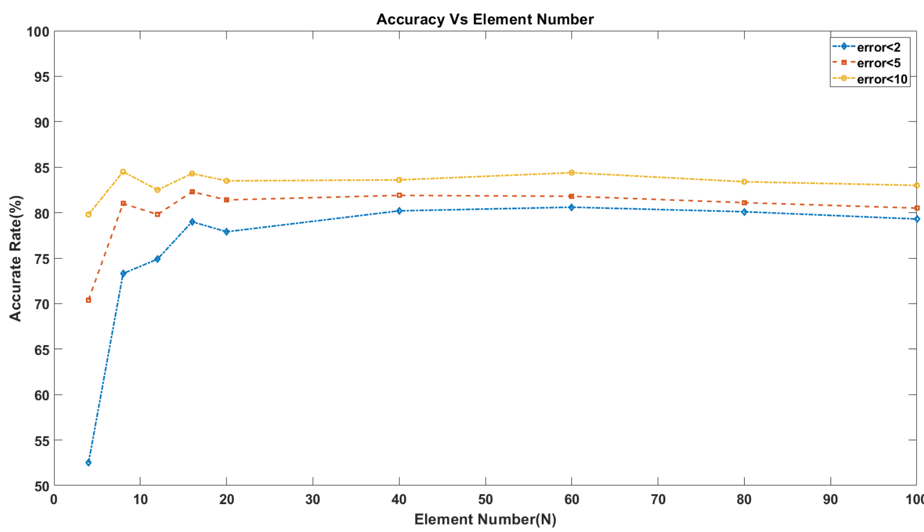

Figure 4.4: Element number vs. accuracy

4.2.4 Element Spacing

Element spacing is also a key factor that is capable of changing the accuracy of the DOA estimation. In past research, the distance between antennas was mostly set to half wavelength [52–71]. However, during our simulation, the result shows that the 0.5λ is not the best solution. Instead, increasing the element distance to the range between

Element Number	Accuracy($< 2°$)	Accuracy($< 5°$)	Accuracy($< 10°$)
4	52.5	70.4	79.8
8	73.3	81	84.5
12	74.9	79.8	82.5
16	79	82.3	84.3
20	77.9	81.4	83.5
40	80.2	81.9	83.6
60	80.6	81.8	84.4
80	80.1	81.1	83.4
100	79.3	80.5	83

Table 4.2: Element number vs. accuracy

0.5λ and 1 λ has a very significant improvement in the resolution, thus increasing the accuracy of DOA estimation, as shown in figure 4.5. For $error < 2°$, the accuracy was increased from 64.5% to 75.1% at the saturation point 0.75λ. The simulation results are also provided in table 4.3 below.

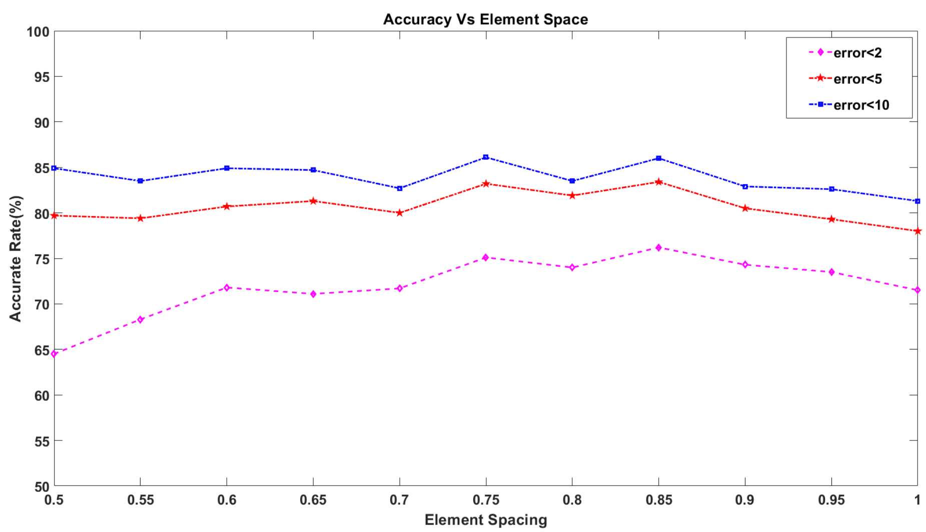

Figure 4.5: Element spacing vs. accuracy

Element Spacing	Accuracy($< 2°$)	Accuracy($< 5°$)	Accuracy($< 10°$)
0.5λ	64.5	79.7	84.9
0.55λ	68.3	79.4	83.5
0.6λ	71.8	80.7	84.9
0.65λ	71.1	81.3	84.7
0.7λ	71.7	80.0	82.7
0.75λ	75.1	83.2	86.1
0.8λ	74.0	81.9	83.5
0.85λ	76.2	83.4	86.0
0.9λ	74.3	80.5	82.9
0.95λ	73.5	79.3	82.6
1λ	71.5	78.0	81.3

Table 4.3: Element spacing vs. accuracy

4.2.5 SNR

Another critical factor is the signal to noise ratio(SNR). As an essential role in all aspects of the signal processing area, SNR shows the most considerable improvement during this simulation. As shown in figure 4.6, increasing the SNR caused a rapid increase in the accuracy level. As the SNR increased from $-21dB$, the accuracy was increased from 12% to 70.4% at the saturation point $-9dB$. The simulation results are also provided in table 4.4.

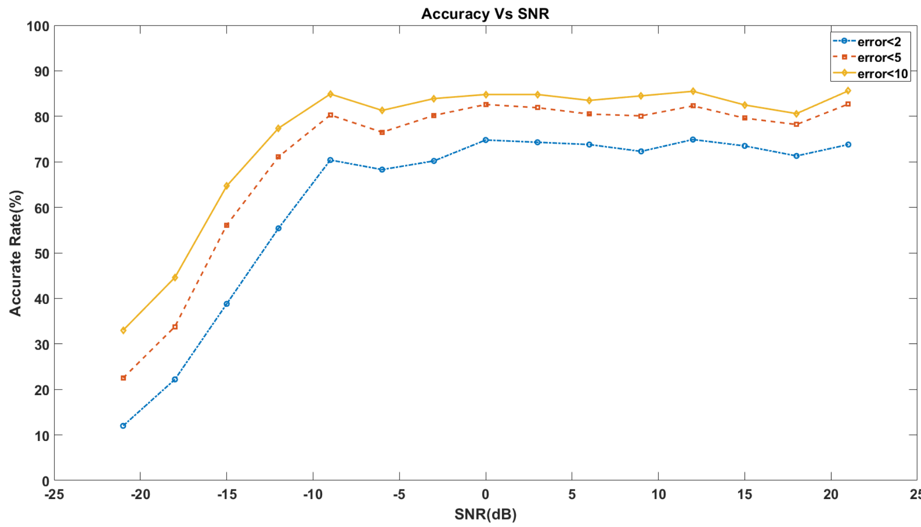

Figure 4.6: SNR vs. accuracy

SNR	Accuracy($< 2°$)	Accuracy($< 5°$)	Accuracy($< 10°$)
-21 dB	12	22.5	33
-18 dB	22.2	33.8	44.6
-15 dB	38.8	56.1	64.7
-12 dB	55.4	71.1	77.4
-9 dB	70.4	80.3	84.9
-6 dB	68.3	76.5	81.3
-3 dB	70.2	80.2	83.9
0 dB	74.8	82.6	84.8
3 dB	74.3	81.9	84.8
6 dB	73.8	80.5	83.5
9 dB	72.3	80.1	84.5
12 dB	74.9	82.3	85.5
15 dB	73.5	79.6	82.5
18 dB	71.8	78.2	80.6
21 dB	73.8	82.7	85.6

Table 4.4: SNR vs. accuracy

4.2.6 Result Analysis

Though increasing the parameter mentioned above improved the accuracy of DOA estimation, the saturation points in these results are hard to ignore. Since the element spacing and number mainly affect the beamforming pattern, therefore, two more simulations have been performed to determine how these two factors will change the beamforming.

4.2.6.1 Element Spacing

Figure 4.7 below shows the gain pattern of a Uniform Linear Array (ULA) with different element spacing. As it shows, when the distance between antennas increases from 0.5λ to 1λ, the main lobe becomes narrower. This will cause an increase in resolution, thus improving the accuracy of the DOA estimation since this will improve the capability of distinguishing multiple signals in a smaller range for DOA algorithms. However, we can see that there is no significant change in the main lobe's width between 0.75λ and 0.95λ; a sub-lobe is becoming more robust than the main lobe, which might be the reason that the simulation shows a saturation point at 0.75λ. Also, the simulation did not include element spacing over 1λ because once it exceeds one wavelength, the sub-lobe becomes more robust than the main lobe, which will result in DOA algorithms giving an incorrect result and degrading the accuracy of the estimations. Interested readers should note that the simulation result includes accuracy when the element spacing over one wavelength has been posted in figure 4.9.

4.2.6.2 Element Number

Figure 4.8 below shows the gain pattern of a Uniform Linear Array (ULA) with different element numbers. As it shows, when the number of elements on the array increases from 4 to 16, the main lobe becomes narrower. Unlike the element spacing, the main lobe's width continues decreasing when the number of elements is increasing. As mentioned above, decreasing the lobe width can improve the accuracy of the DOA algorithm. Therefore, the DOA algorithm's accuracy should keep increasing with the element number;however, this does not match the simulation result. One possible reason for this phenomenon is that the resolution of DOA algorithms has a maximum defined by other variables. Once the element number exceeds this limitation, increasing it further cannot provide further improvement.

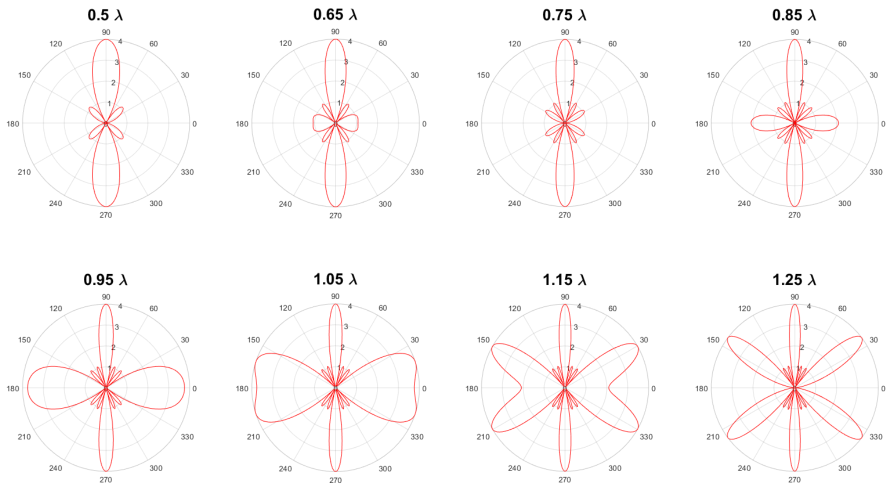

Figure 4.7: Beamforming pattern for different element spacing

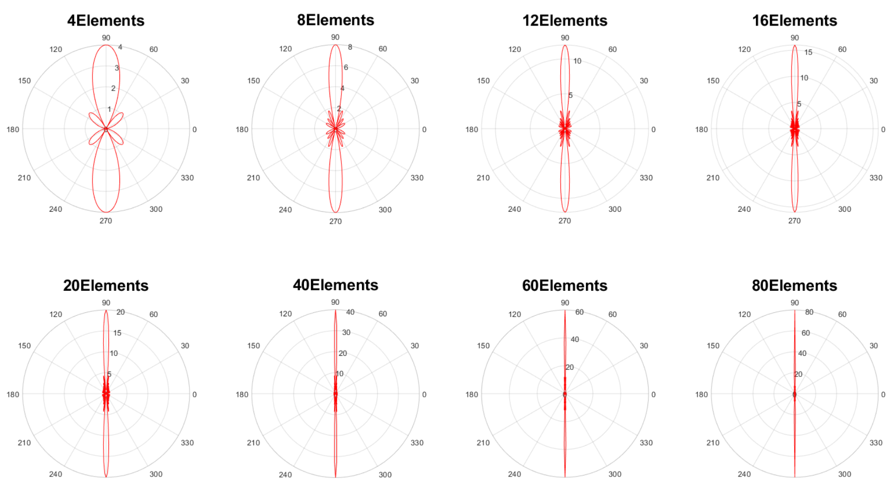

Figure 4.8: Beamforming pattern for different number of elements

4.2.7 Accuracy Prediction

As described above, increasing the element number and inter-element distance of the antenna array will narrow its half-power beamwidth. This effect can be described as

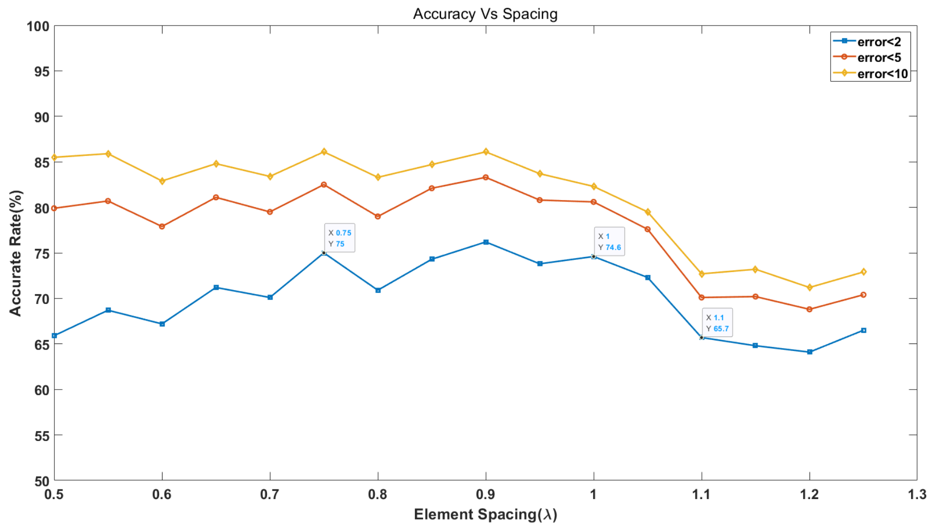

Figure 4.9: Element spacing vs. accuracy from 0.5λ to 1.25λ

below:

$$HPBW = \theta = 0.89 * \frac{\lambda}{D} \tag{4.2}$$

where D is the aperture size of the array. Therefore, the half-power beamwidth can be described as:

$$\theta = 0.89 * \frac{\lambda}{N * d * \lambda} = 0.89 * \frac{1}{N * d} \tag{4.3}$$

As mentioned at the beginning, the accuracy is defined as a probability that the DOA estimation result has a certain threshold which can be described as:

$$P_{accurate} = 1 - P_{incorrect} \tag{4.4}$$

In order to calculate $P_{incorrect}$, we need to consider two different scenarios: either the interference signal is located too close to the desired signal(in other words, there are two signals in the same beamwidth) or there is an interference signal that is not in the same beamwidth with the desired signal but has a higher power. Assume that the desired signal S_1 is located at $\phi_1 = 45°$ and the beamwidth of the array is θ. The first situation will happen when there is a interference signal S_2 located at $45 - \theta < \phi_2 < 45 + \theta$, with a random amplification factor $0.1 < A < 1.2$. Then the probability for the first scenario can be written as:

$$P_1 = \frac{2\theta}{0.5\pi} \tag{4.5}$$

For the second scenario,the probability can be calculated as below:

$$P_2 = P(\phi_2 > \phi_1 + \theta \cap \phi_2 < \phi_1 - \theta) * P(A > 1) \tag{4.6}$$

$$P_2 = (1 - \frac{2\theta}{0.5\pi}) * P(A > 1) \tag{4.7}$$

$$P_{incorrect} = P_1 + P_2 \tag{4.8}$$

Then the accuracy can be written as:

$$P_{accurate} = 1 - [\frac{2\theta}{0.5\pi} + (1 - \frac{2\theta}{0.5\pi}) * P(A > 1)] \tag{4.9}$$

4.2.7.1 Simulation Result

Since the function that describes the relationship between antenna number N and inter-element distance d was found, a series of simulations were performed to validate the function. The results have been posted below. Figures 4.10 to 4.12 are the predicted and simulated accuracy for different inter-element distances when antenna number $N = 4, 6, 8$. Figure 4.13 shows the predicted and simulated accuracy for different element number N when inter-element distance $d = 0.75\lambda$

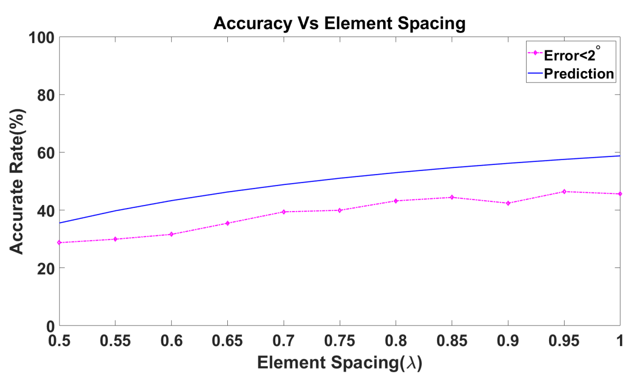

Figure 4.10: Accuracy vs. inter-element distance ($N = 4$)

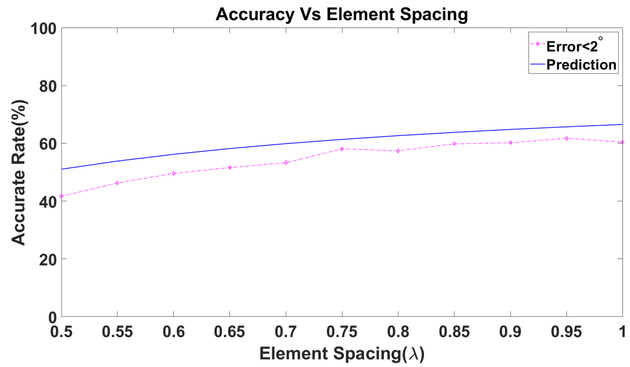

Figure 4.11: Accuracy vs. inter-element distance ($N = 6$)

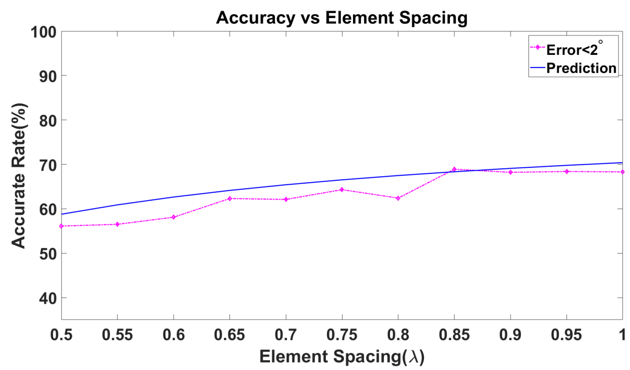

Figure 4.12: Accuracy vs. inter-element distance ($N = 8$)

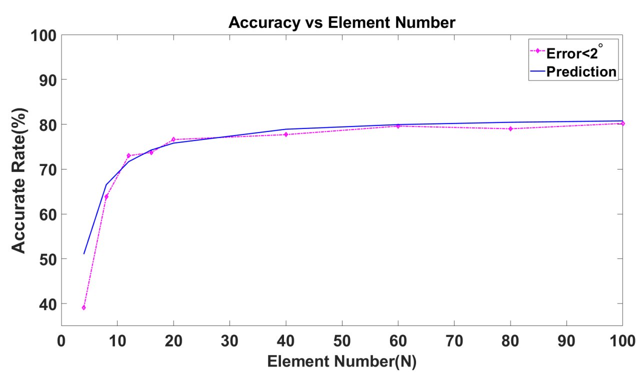

Figure 4.13: Accuracy vs. number of elements

4.3 Virtual Array Expansion Based on Linear Prediction

For further improvement of the DOA based indoor localization system, we decided to upgrade the proposed system into a 2-D DOA spectrum. In this way, the system does not require a geometry calculation with two different DOA, thus saving time and space of the proposed system. However, to create a 2-D DOA spectrum, it is required for the system to have a uniform rectangular array (URA) with at least 16 antennas (4*4). This requirement is hard to implement in the real-world since most commercial RF receivers can only provide four channels. To achieve 16 channels, we need to synchronize 4 receivers; this is against the principle of this project, which is to create a system that can be easily deployed.

An alternative solution to the problem is the array expansion method [72–77].In this project, we decide to use the linearly predicted array expansion method which introduced by Sim [78] for high efficiency. This method's basic idea is to extract the linear relationship among signals received by the antennas and use it to generate extrapolated signal outside the array antenna, which can be expressed as

$$\boldsymbol{X}_n = [\boldsymbol{X}_1, \boldsymbol{X}_2, ..., \boldsymbol{X}_{n-1}] * \boldsymbol{\mu}_f \tag{4.10}$$

where $\boldsymbol{\mu}_f$ is the coefficients for the linear combination. By solving the least square problem, the coefficients can be expressed as

$$\boldsymbol{\mu}_f^* = \text{argmin} \left\| \boldsymbol{X}_n - \widetilde{\boldsymbol{X}_n} \right\|_2^2 \tag{4.11}$$

which minimized the error between the actual received signal and the predicted signal. Using the linear least squares method, μ_f^* can be calculated as

$$\boldsymbol{\mu}_f^* = \boldsymbol{X}_f^H (\boldsymbol{X}_f \boldsymbol{X}_f^H)^{-1} \boldsymbol{X}_n \tag{4.12}$$

Following Sim's work, by using this coefficient, the linearly predicted array expansion can be conducted to extrapolate the signal.

To construct a 4-by-4 URA using linearly predicted array expansion, an L-shape phased array, as shown in figure 4.14, is needed. The seven red antennas in the figure are the physical antennas used; The blue ones are the virtual expanded antennas. The

Figure 4.14: Virtual URA layout

procedure using linear predict array expansion can be expressed in the following steps. Assume E22 is the virtual antenna that we want to expand. First, use signals received from E11 and E12 to extract linear coefficient μ_f between these two antennas. Second, use the received signal from antenna E21 as the reference to predict the signal received by E22. The process of signal generation can be expressed as

$$\boldsymbol{x}_{22} = \boldsymbol{x}_{21} * \mu_f^* \tag{4.13}$$

By repeating the same procedure, we can generate the signal for all virtual antennas. However, signals generated by this procedure have only vertical phase information since signals are generated using only linear coefficient on vertical antennas. To solve this, all virtual signals are generated again, but this time reference signals will be signals received on the vertical array (E12 to E14), and the linear coefficient will be extracted on the horizontal antenna. Then, by superposition of two signals, the signal for the virtual antenna could be generated correctly.

To evaluate the effectiveness of this method, we simulated this with Matlab. For comparison, the 2-D spatial spectrum for a physical 4-by-4 URA has also been estimated. In this simulation, two signal sources were placed at (0,0) and (45,45) degrees. The SNR of signals received by array was set to 20 dB. The result shows that the proposed method performs 2-D DOA estimation with only an L-shaped antenna array. As shown in the figure 4.15, the two spatial spectra both show two peaks around desired locations. Since

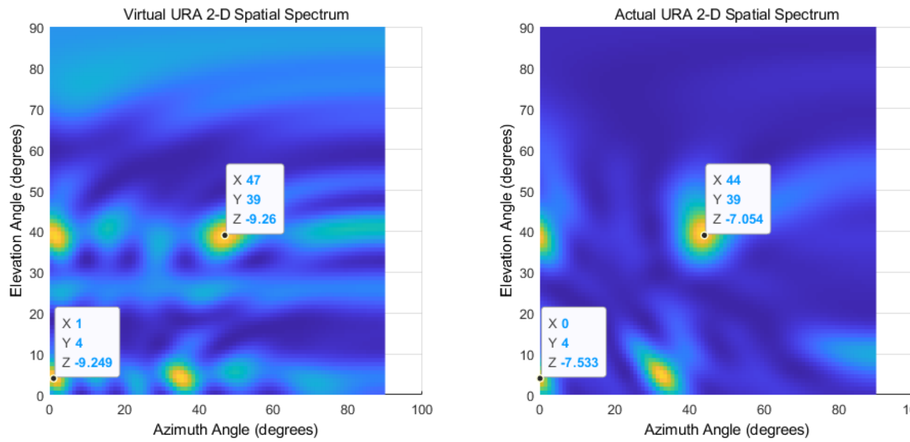

Figure 4.15: 2D spatial spectrum for virtual and physical URA

the actual URA structure is hard to implement, the proposed technique has not been evaluated in the real world.

4.4 Multipath Effect Cancellation

As mentioned earlier, the multipath effect plays a vital role in degrading the performance of DOA estimations. Once the multipath signal can be recognized or eliminated, the performance of DOA estimation can be rapidly improved. In past research, some least square method based multipath cancellation methods were proposed [79–81]. However, these methods require additional calculation. Thus, we decided to find a way to remove the multipath effect as much as possible without requiring additional calculation. Since the multipath signal has a time delay compared to the direct path signal, we decided to combine a sinusoidal wave with a period of silence with the same length to create a waveform, as figure 4.16 shows. The basic idea of this method is that since the multipath signal has a time delay, it has a considerable chance to superposition on the silence period; thus, it is possible to distinguish direct and multipath signals and eventually remove multipath effect in the DOA estimation.

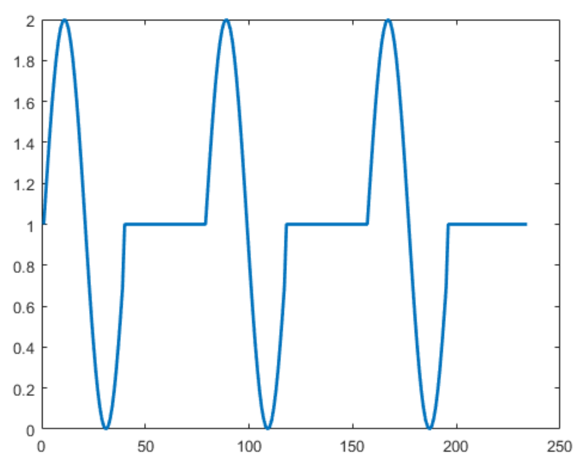

Figure 4.16: Proposed multipath cancelling waveform

To evaluate this idea's performance, the proposed waveform has been simulated in several different situations and compared with both sinusoidal and wideband Wi-Fi signals. We simulated the performance of the proposed signal when three different signal sources are located at 5, 20, and 35 degrees. Simulation results in figure 4.17 show that compared with the sinusoidal and wideband signal, the proposed signal has a higher resolution and accuracy.

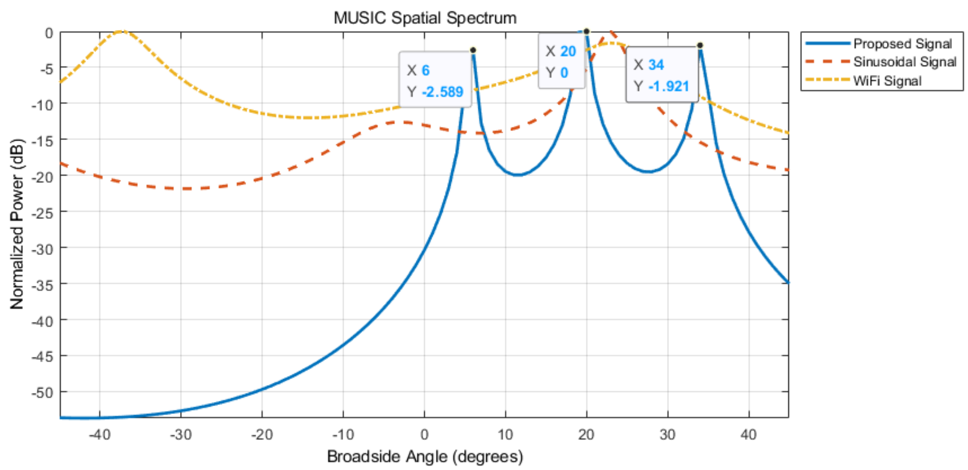

Figure 4.17: MUSIC estimation performance comparison

Since the simulation result above shows an outplaying performance on DOA estimation, we decided to apply it to 2D DOA estimation. In this simulation, the signal sources are placed at (15,15), (60,5) and (33,51). As shown in figure 4.18 and figure 4.19, the proposed signal massively improved the resolution of the 2D DOA estimation. Also, unlike sinusoidal and wideband Wi-Fi signals, the proposed signal can distinguish three different signal sources and detect them accurately.

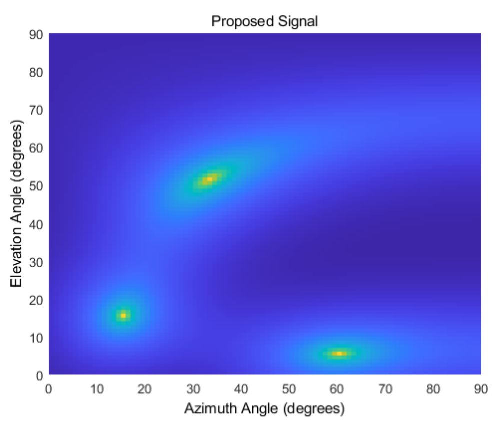

Figure 4.18: 2D MUSIC estimation using proposed signal

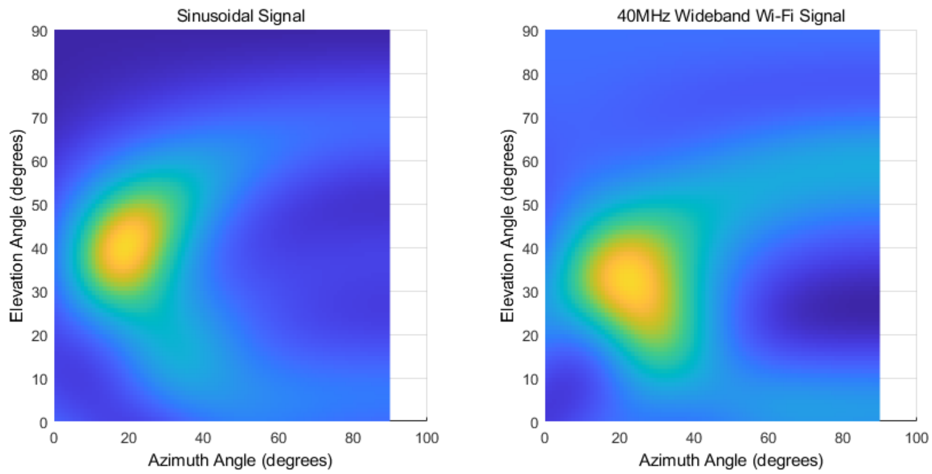

Figure 4.19: 2D MUSIC estimation using Sinusoidal and WiFi signal

4.5 Effectiveness

In this section, we proposed a series of enhancement and refinement methods. The first two methods have already been deployed in a real-world experiment, and the result matches the expectation. The third and fourth methods have not been tested in the real world due to infrastructure limitations and the impact of COVID-19. For this reason, we yet cannot evaluate their effectiveness in the real world. Also, one thing needs to be clarified: although the third and fourth methods showed excellent performance individually in simulation, they cannot work correctly once combined.

Chapter 5: Future Work

For further improvement of this project, both hardware and algorithms will be refined to increase the accuracy of the current system. For the hardware aspect, both antenna array and receiver can be improved to provide better performance than the current stage. For example, currently the antenna arrays are the production of handcraft; this significantly degraded the ULA's performance and added more random error to the array. In further experiments, the array element should be carefully selected and assembled on a 3D printed holder and calibrated before attaching it to the receiver. For the algorithm aspect, the current algorithm can be improved with statistic structure and a more robust DOA estimation algorithm that can provide either better resolution or faster response.

For statistics, a Kalman filter can be infused with the Bartlett algorithm.The Kalman filter, which was first introduced in 1960 by Rudolf Emil Kalman, is claimed to be an optimal estimator. It optimally estimates the system's error covariance and recursively uses prediction to improve system measurement from time to time [82–84]. For this project, the Kalman filter can help the system correct DOA estimation.

For the algorithm aspect, since in chapter 6, we proposed a method that may be capable of distinguishing multiple signals, the best direction of developing a new DOA estimation algorithm would be less calculation complexity, thus improving the response time of the system to achieve a real-time level estimation rate.

Also, as mentioned in chapter 6, some refinement and enhancement methods have not been tested in the experiment yet. Therefore, in the future, these methods should be tested once the infrastructures can perform experiments. Additionally, these experiments may help us find a solution to combining refinements 3 and 4 together.

Chapter 6: Conclusion

In this paper, we aimed to design an indoor localization system with a compact size and sub-meter level accuracy by using existing signal in the environment. Using a Bartlett base algorithm, we successfully acquired the target emitter's location with an average accuracy of 50 centimetres but maximum error greater than the preferred error threshold. To decrease error level, optimizations of algorithm and system structure are proposed for future implementation. In particular, we suggest implementing the Kalman filter to the algorithm and applying the linear array expansion technique to the antenna array. However, these methods can only be used after the functionality of these methods are verified

Bibliography

[1] R. Ye, S. Redfield, and H. Liu, "High-precision indoor uwb localization: Technical challenges and method," in *2010 IEEE International Conference on Ultra-Wideband*, vol. 2. IEEE, 2010, pp. 1–4.

[2] Z. Su, G. Shao, and H. Liu, "Semidefinite programming for nlos error mitigation in tdoa localization," *IEEE Communications Letters*, vol. 22, no. 7, pp. 1430–1433, 2017.

[3] S. Zhao and H. Liu, "On the optimum linear receiver for impulse radio systems in the presence of pulse overlapping," *IEEE Communications Letters*, vol. 9, no. 4, pp. 340–342, 2005.

[4] ——, "Prerake diversity combining for pulsed uwb systems considering realistic channels with pulse overlapping and narrow-band interference," in *GLOBECOM'05. IEEE Global Telecommunications Conference, 2005.*, vol. 6. IEEE, 2005, pp. 5–pp.

[5] Y. Zou, H. Liu, W. Xie, and Q. Wan, "Semidefinite programming methods for alleviating sensor position error in tdoa localization," *IEEE Access*, vol. 5, pp. 23 111–23 120, 2017.

[6] T. Qiao and H. Liu, "Improved least median of squares localization for non-line-of-sight mitigation," *IEEE communications letters*, vol. 18, no. 8, pp. 1451–1454, 2014.

[7] ——, "An improved method of moments estimator for toa based localization," *IEEE communications letters*, vol. 17, no. 7, pp. 1321–1324, 2013.

[8] T. Qiao, S. Redfield, A. Abbasi, Z. Su, and H. Liu, "Robust coarse position estimation for tdoa localization," *IEEE Wireless Communications Letters*, vol. 2, no. 6, pp. 623–626, 2013.

[9] Y. Zou, H. Liu, and Q. Wan, "Joint synchronization and localization in wireless sensor networks using semidefinite programming," *IEEE Internet of Things Journal*, vol. 5, no. 1, pp. 199–205, 2017.

[10] ——, "An iterative method for moving target localization using tdoa and fdoa measurements," *IEEE Access*, vol. 6, pp. 2746–2754, 2017.

[11] Y. Jang, H. Lim, and D. Yoon, "Multipath effect on radar detection of nonfluctuating targets," *IEEE Transactions on Aerospace and Electronic Systems*, vol. 51, no. 1, pp. 792–795, 2015.

[12] F. Zafari, A. Gkelias, and K. K. Leung, "A survey of indoor localization systems and technologies," *IEEE Communications Surveys & Tutorials*, vol. 21, no. 3, pp. 2568–2599, 2019.

[13] N. U. Hassan, A. Naeem, M. A. Pasha, T. Jadoon, and C. Yuen, "Indoor positioning using visible led lights: A survey," *ACM Computing Surveys (CSUR)*, vol. 48, no. 2, pp. 1–32, 2015.

[14] T. Sanpechuda and L. Kovavisaruch, "A review of rfid localization: Applications and techniques," in *2008 5th international conference on electrical engineering/electronics, computer, telecommunications and information technology*, vol. 2. IEEE, 2008, pp. 769–772.

[15] H. Xu, M. Wu, P. Li, F. Zhu, and R. Wang, "An rfid indoor positioning algorithm based on support vector regression," *Sensors*, vol. 18, no. 5, p. 1504, 2018.

[16] J. Zhou, K.-K. Chu, and J.-Y. Ng, "Providing location services within a radio cellular network using ellipse propagation model," in *19th International Conference on Advanced Information Networking and Applications (AINA'05) Volume 1 (AINA papers)*, vol. 1. IEEE, 2005, pp. 559–564.

[17] S.-H. Fang, C.-H. Wang, T.-Y. Huang, C.-H. Yang, and Y.-S. Chen, "An enhanced zigbee indoor positioning system with an ensemble approach," *IEEE Communications Letters*, vol. 16, no. 4, pp. 564–567, 2012.

[18] M. F. Mansour and D. W. Waters, "Uncensored indoor positioning," *IEEE Signal Processing Letters*, vol. 21, no. 7, pp. 824–828, 2014.

[19] A. Zhang, Y. Yuan, Q. Wu, S. Zhu, and J. Deng, "Wireless localization based on rssi fingerprint feature vector," *International Journal of Distributed Sensor Networks*, vol. 11, no. 11, p. 528747, 2015.

[20] H. Liu, H. Darabi, P. Banerjee, and J. Liu, "Survey of wireless indoor positioning techniques and systems," *IEEE Transactions on Systems, Man, and Cybernetics, Part C (Applications and Reviews)*, vol. 37, no. 6, pp. 1067–1080, 2007.

[21] B. T. Fang *et al.*, "Simple solutions for hyperbolic and related position fixes," *IEEE transactions on aerospace and electronic systems*, vol. 26, no. 5, pp. 748–753, 1990.

[22] M. Kanaan and K. Pahlavan, "A comparison of wireless geolocation algorithms in the indoor environment," in *2004 IEEE Wireless Communications and Networking Conference (IEEE Cat. No. 04TH8733)*, vol. 1. IEEE, 2004, pp. 177–182.

[23] R. C. Qiu, H. Liu, and X. Shen, "Ultra-wideband for multiple access communications," *IEEE Communications Magazine*, vol. 43, no. 2, pp. 80–87, 2005.

[24] H. Liu, "Error performance of a pulse amplitude and position modulated ultra-wideband system over lognormal fading channels," *IEEE Communications Letters*, vol. 7, no. 11, pp. 531–533, 2003.

[25] H. Liu, R. C. Qiu, and Z. Tian, "Error performance of pulse-based ultra-wideband mimo systems over indoor wireless channels," *IEEE Transactions on Wireless Communications*, vol. 4, no. 6, pp. 2939–2944, 2005.

[26] H. Liu, "Multicode ultra-wideband scheme using chirp waveforms," *IEEE Journal on selected areas in communications*, vol. 24, no. 4, pp. 885–891, 2006.

[27] S. Zhao, H. Liu, and Z. Tian, "Decision directed autocorrelation receivers for pulsed ultra-wideband systems," *IEEE Transactions on Wireless Communications*, vol. 5, no. 8, pp. 2175–2184, 2006.

[28] ——, "A decision-feedback autocorrelation receiver for pulsed ultra-wideband systems," in *Proceedings. 2004 IEEE Radio and Wireless Conference (IEEE Cat. No. 04TH8746)*. IEEE, 2004, pp. 251–254.

[29] S. Zhao and H. Liu, "Transmitter-side multipath preprocessing for pulsed uwb systems considering pulse overlapping and narrow-band interference," *IEEE transactions on vehicular technology*, vol. 56, no. 6, pp. 3502–3510, 2007.

[30] S. Zhao, P. Orlik, A. F. Molisch, H. Liu, and J. Zhang, "Hybrid ultrawideband modulations compatible for both coherent and transmit-reference receivers," *IEEE transactions on wireless communications*, vol. 6, no. 7, pp. 2551–2559, 2007.

[31] C. Drane, M. Macnaughtan, and C. Scott, "Positioning gsm telephones," *IEEE Communications magazine*, vol. 36, no. 4, pp. 46–54, 1998.

[32] S. Chen, X. Li, and Z. Shao, "Study on the performance of doa estimation algorithms," in *2015 IEEE International Conference on Communication Problem-Solving (ICCP)*. IEEE, 2015, pp. 475–477.

[33] S. Zhang, D. Xu, and Y. Li, "Comparison of several doa methods based on spatial spectrum estimation," in *2017 International Conference on Computer Technology, Electronics and Communication (ICCTEC)*. IEEE, 2017, pp. 145–148.

[34] Y. Xiao, J. Yin, H. Qi, H. Yin, and G. Hua, "Mvdr algorithm based on estimated diagonal loading for beamforming," *Mathematical Problems in Engineering*, vol. 2017, 2017.

[35] F. Akbari, S. S. Moghaddam, and V. T. Vakili, "Music and mvdr doa estimation algorithms with higher resolution and accuracy," in *2010 5th International Symposium on Telecommunications*. IEEE, 2010, pp. 76–81.

[36] K. Niwaria, M. Jain *et al.*, "A literature survey different algorithms of music and mvdr doa estimation," *International Journal of Engineering and Management Research (IJEMR)*, vol. 8, no. 2, pp. 56–60, 2018.

[37] O. A. Oumar, M. F. Siyau, and T. P. Sattar, "Comparison between music and esprit direction of arrival estimation algorithms for wireless communication systems," in *The First International Conference on Future Generation Communication Technologies*. IEEE, 2012, pp. 99–103.

[38] Y.-Y. Dong, C.-x. Dong, Z.-b. Shen, and G.-q. Zhao, "Conjugate augmented spatial temporal technique for 2-d doa estimation with l-shaped array," *IEEE Antennas and Wireless Propagation Letters*, vol. 14, pp. 1622–1625, 2015.

[39] M. Gialich, A. Im, T. Lee, Z. Aliyazicioglu, and H. Hwang, "Doa estimation using array antenna with large inter-element spacing," in *2012 IEEE 11th International Conference on Signal Processing*, vol. 3. IEEE, 2012, pp. 1701–1704.

[40] V. Krishnaveni, T. Kesavamurthy, and B. Aparna, "Beamforming for direction-of-arrival (doa) estimation-a survey," *International Journal of Computer Applications*, vol. 61, no. 11, 2013.

[41] H. Chen, S.-C. Chan, Z. Zhang, and K.-L. Ho, "Adaptive beamforming and recursive doa estimation using frequency-invariant uniform concentric spherical arrays," *IEEE Transactions on Circuits and Systems I: Regular Papers*, vol. 55, no. 10, pp. 3077–3089, 2008.

[42] R. Schmidt, "Multiple emitter location and signal parameter estimation," *IEEE transactions on antennas and propagation*, vol. 34, no. 3, pp. 276–280, 1986.

[43] R. Roy and T. Kailath, "Esprit-estimation of signal parameters via rotational invariance techniques," *IEEE Transactions on acoustics, speech, and signal processing*, vol. 37, no. 7, pp. 984–995, 1989.

[44] W. Wang, X. Wang, H. Song, and Y. Ma, "Conjugate esprit for doa estimation in monostatic mimo radar," *Signal Processing*, vol. 93, no. 7, pp. 2070–2075, 2013.

[45] J. Lin, X. Ma, S. Yan, and C. Hao, "Time-frequency multi-invariance esprit for doa estimation," *IEEE Antennas and Wireless Propagation Letters*, vol. 15, pp. 770–773, 2015.

[46] X. Zhang, X. Gao, and D. Xu, "Multi-invariance esprit-based blind doa estimation for mc-cdma with an antenna array," *IEEE Transactions on Vehicular Technology*, vol. 58, no. 8, pp. 4686–4690, 2009.

[47] F.-M. Han and X.-D. Zhang, "An esprit-like algorithm for coherent doa estimation," *IEEE Antennas and Wireless Propagation Letters*, vol. 4, pp. 443–446, 2005.

[48] J. Li, D. Jiang, and X. Zhang, "Doa estimation based on combined unitary esprit for coprime mimo radar," *IEEE Communications Letters*, vol. 21, no. 1, pp. 96–99, 2016.

[49] J. Capon, "High-resolution frequency-wavenumber spectrum analysis," *Proceedings of the IEEE*, vol. 57, no. 8, pp. 1408–1418, 1969.

[50] L. Zhao, H. Liu, Y. Li, and Y. Zhou, "Doa estimation under sensor gain and phase uncertainties," in *2015 International Conference on Estimation, Detection and Information Fusion (ICEDIF)*. IEEE, 2015, pp. 209–213.

[51] A. C. Clay, S.-C. Wooh, L. Azar, and J.-Y. Wang, "Experimental study of phased array beam steering characteristics," *Journal of Nondestructive Evaluation*, vol. 18, no. 2, pp. 59–71, 1999.

[52] L. Xiaozhi, S. Muye, and Y. Yinghua, "An effective doa estimation method of coherent signals based on reconstruct weighted noise subspace," in *2017 29th Chinese Control And Decision Conference (CCDC)*. IEEE, 2017, pp. 2218–2222.

[53] M. Pesavento and A. B. Gershman, "Maximum-likelihood direction-of-arrival estimation in the presence of unknown nonuniform noise," *IEEE Transactions on Signal Processing*, vol. 49, no. 7, pp. 1310–1324, 2001.

[54] Y. Zhang, Z. Ye, X. Xu, and N. Hu, "Off-grid doa estimation using array covariance matrix and block-sparse bayesian learning," *Signal Processing*, vol. 98, pp. 197–201, 2014.

[55] S. Yan, "Broadband beamspace doa estimation: Frequency-domain and time-domain processing approaches," *EURASIP Journal on Advances in Signal Processing*, vol. 2007, no. 1, p. 016907, 2006.

[56] Z. Zhang, P. Wei, L. Deng, and H. Zhang, "Joint estimation of doa and frequency with sub-nyquist sampling in a binary array radar system," in *2019 IEEE Radar Conference (RadarConf)*. IEEE, 2019, pp. 1–6.

[57] H. Zeng, Z. Ahmad, J. Zhou, Q. Wang, and Y. Wang, "Doa estimation algorithm based on adaptive filtering in spatial domain," *China Communications*, vol. 13, no. 12, pp. 49–58, 2016.

[58] J. Li, F. Wang, and D. Jiang, "Direction of arrival estimation using sum co-array of coprime arrays," in *2017 International Applied Computational Electromagnetics Society Symposium (ACES)*. IEEE, 2017, pp. 1–2.

[59] Z.-Q. He, Z.-P. Shi, and L. Huang, "Covariance sparsity-aware doa estimation for nonuniform noise," *Digital Signal Processing*, vol. 28, pp. 75–81, 2014.

[60] Y. Zhang and Z. Ye, "Efficient method of doa estimation for uncorrelated and coherent signals," *IEEE Antennas and Wireless Propagation Letters*, vol. 7, pp. 799–802, 2008.

[61] L. Nagy and Z. Szalay, "Radar target as distributed source for doa estimation," in *The 8th European Conference on Antennas and Propagation (EuCAP 2014)*. IEEE, 2014, pp. 2323–2327.

[62] Z. Chen and J. Wang, "Es-dpr: A doa-based method for passive localization in indoor environments," *Sensors*, vol. 19, no. 11, p. 2482, 2019.

[63] Z. Zhang, C. Zhou, Y. Gu, J. Zhou, and Z. Shi, "An idft approach for coprime array direction-of-arrival estimation," *Digital Signal Processing*, vol. 94, pp. 45–55, 2019.

[64] X. Dai, X. Zhang, and Y. Wang, "Extended doa-matrix method for doa estimation via two parallel linear arrays," *IEEE Communications Letters*, vol. 23, no. 11, pp. 1981–1984, 2019.

[65] H. L. Van Trees, "Optimum array processing: Part iv of detection," *Estimation, and Modulation Theory*, 2002.

[66] A. Vesa and A. Iozsa, "Direction-of-arrival estimation for uniform sensor arrays," in *2010 9th International Symposium on Electronics and Telecommunications*. IEEE, 2010, pp. 249–252.

[67] L. Bai, C.-Y. Peng, and S. Biswas, "Association of doa estimation from two ulas," *IEEE Transactions on Instrumentation and Measurement*, vol. 57, no. 6, pp. 1094–1101, 2008.

[68] S. Shirvani-Moghaddam and F. Akbari, "A novel ula-based geometry for improving aoa estimation," *EURASIP Journal on Advances in Signal Processing*, vol. 2011, no. 1, p. 39, 2011.

[69] Y. Zhang, X. Xu, Y. A. Sheikh, and Z. Ye, "A rank-reduction based 2-d doa estimation algorithm for three parallel uniform linear arrays," *Signal Processing*, vol. 120, pp. 305–310, 2016.

[70] J. Li, X. Zhang, and H. Chen, "Improved two-dimensional doa estimation algorithm for two-parallel uniform linear arrays using propagator method," *Signal Processing*, vol. 92, no. 12, pp. 3032–3038, 2012.

[71] J. Zhang, D. Huang, H. Cai, and P. Huang, "High-resolution and steady doa estimation based on reconstruction matrix," in *2010 3rd International Conference on Computer Science and Information Technology*, vol. 7. IEEE, 2010, pp. 216–220.

[72] A. Moffet, "Minimum-redundancy linear arrays," *IEEE Transactions on antennas and propagation*, vol. 16, no. 2, pp. 172–175, 1968.

[73] M. Ishiguro, "Minimum redundancy linear arrays for a large number of antennas," *Radio Science*, vol. 15, no. 6, pp. 1163–1170, 1980.

[74] P. Pal and P. Vaidyanathan, "Nested arrays in two dimensions, part ii: Application in two dimensional array processing," *IEEE Transactions on Signal Processing*, vol. 60, no. 9, pp. 4706–4718, 2012.

[75] P. Pal and P. P. Vaidyanathan, "Nested arrays: A novel approach to array processing with enhanced degrees of freedom," *IEEE Transactions on Signal Processing*, vol. 58, no. 8, pp. 4167–4181, 2010.

[76] P. P. Vaidyanathan and P. Pal, "Sparse sensing with co-prime samplers and arrays," *IEEE Transactions on Signal Processing*, vol. 59, no. 2, pp. 573–586, 2010.

[77] Z. Tan, Y. C. Eldar, and A. Nehorai, "Direction of arrival estimation using co-prime arrays: A super resolution viewpoint," *IEEE Transactions on Signal Processing*, vol. 62, no. 21, pp. 5565–5576, 2014.

[78] H. Sim, S. Lee, S. Kang, and S.-C. Kim, "Enhanced doa estimation using linearly predicted array expansion for automotive radar systems," *IEEE Access*, vol. 7, pp. 47 714–47 727, 2019.

[79] K. Wang, R. Tao, Y. Ma, and T. Shan, "Adaptive multipath cancellation algorithm in passive radar," in *2006 CIE International Conference on Radar*. IEEE, 2006, pp. 1–4.

[80] J. E. Piper, "Multipath cancellation in the time domain," in *OCEANS 2010 MTS/IEEE SEATTLE*. IEEE, 2010, pp. 1–4.

[81] F. J. Álvarez, T. Aguilera, and R. López-Valcarce, "Cdma-based acoustic local positioning system for portable devices with multipath cancellation," *Digital Signal Processing*, vol. 62, pp. 38–51, 2017.

[82] M. Hawes, L. Mihaylova, F. Septier, and S. Godsill, "A bayesian compressed sensing kalman filter for direction of arrival estimation," in *2015 18th International Conference on Information Fusion (Fusion)*. IEEE, 2015, pp. 969–975.

[83] M. VenuMadhava, S. Jagadeesha, and T. Yerriswamy, "A comparitive study of doa estimation algorithms with applications to tracking using kalman filter," *Signal & Image Processing: An International Journal (SIPIJ)*, vol. 6, no. 6, 2015.

[84] D. Pasculli, A. Baruzzi, C. Moscardini, D. Petri, M. Conti, and M. Martorella, "Dvb-t passive radar tracking on real data using extended kalman filter with doa estimation," in *2013 14th International Radar Symposium (IRS)*, vol. 1. IEEE, 2013, pp. 184–189.

[85] L. T. Common, "Propagation losses through common building materials 2.4 ghz vs 5 ghz," *E10589, Magis Network, Inc*, 2002.